

## DETRITAL CLAY COATS, CLAY MINERALS, AND PYRITE: A MODERN SHALLOW-CORE ANALOGUE FOR ANCIENT AND DEEPLY BURIED ESTUARINE SANDSTONES

JOSHUA GRIFFITHS,<sup>1,2</sup> RICHARD H. WORDEN,<sup>1</sup> LUKE J. WOOLDRIDGE,<sup>1,3</sup> JAMES E. P. UTLEY,<sup>1</sup> AND ROBERT A. DULLER<sup>1</sup>

<sup>1</sup>Department of Earth, Ocean and Ecological Sciences, University of Liverpool, Liverpool U.K.

<sup>2</sup>BP Exploration, Chertsey Road, Sunbury-on-Thames, Middlesex, TW16 7LN, U.K.

<sup>3</sup>BP Upstream Technology, Chertsey Road, Sunbury-on-Thames, Middlesex, TW16 7LN, U.K.

e-mail: [joshua.griffiths@BP.com](mailto:joshua.griffiths@BP.com)

**ABSTRACT:** The spatial distribution of clay minerals and authigenic-clay-coated sand grains in ancient and deeply buried petroleum reservoirs, which can enhance or degrade reservoir quality, is poorly understood. Authigenic clay coats are reported to originate from the thermally driven recrystallization of detrital clay coats or through *in situ* growth from the authigenic alteration of precursor and early-diagenetic minerals during burial diagenesis. To help predict the spatial distribution of authigenic clay coats and clay minerals in estuarine sandstones, this study provides the first modern-analogue study, using the Ravenglass Estuary, UK, which integrates the distribution patterns of lithofacies, Fe-sulfide, and precursor detrital-clay-coats and clay-minerals. X-ray-diffraction-determined mineralogy and the extent of detrital clay-coat coverage of sediment in twenty-three one-meter cores was established, at an unprecedented high resolution. The output from this study shows that detrital clay mineral distribution patterns are controlled principally by the physical sorting of clay minerals by grain size. Chlorite is most abundant in coarser-grained sediment (e.g., low-amplitude dunes), whereas illite is most abundant in finer-grained sub-environments (e.g., mud flats). Kaolinite abundance is relatively homogeneous, whereas smectite abundance is negligible in the Ravenglass Estuary. This study has shown that distribution patterns of detrital-clay-coats and clay-minerals are controlled by processes active during deposition and bio-sediment interaction in the top few millimeters in the primary deposition environment. In the Ravenglass Estuary, distribution patterns of detrital-clay-coats and clay-minerals have not been overprinted by the postdepositional processes of sediment bioturbation or mechanical infiltration. Optimum detrital-clay-coat coverage and clay mineralogy, which might serve as a precursor to porosity-preserving authigenic clay coats in deeply buried sandstone reservoirs, is likely to occur in low-amplitude dunes in the inner estuary and central basin. Furthermore, bioturbation in low-amplitude dunes has reduced Fe-sulfide growth due to oxidization, meaning that iron remains available for the formation of authigenic Fe-bearing clay minerals, such as chlorite, that can lead to enhanced reservoir quality in deeply buried sandstones.

### INTRODUCTION

Clay minerals can significantly impact the petrophysical properties (e.g., porosity, permeability, and water saturation) of sandstone reservoirs. For example, pore-filling quartz cement in deeply buried sandstones (> 80 to 100 °C), can be inhibited by authigenic chlorite clay coats (Ehrenberg 1993; Stricker et al. 2016; Skarpeid et al. 2017), while some clay minerals (e.g., illite) can plug pore throats and promote chemical compaction and subsequent quartz cementation (Oelkers et al. 1996; Worden and Morad 2003; Worden et al. 2018). Authigenic clay coats in sandstones have been reported to originate from (i) the thermally driven recrystallization of low-temperature, precursor (before burial) detrital clay coats, and (ii) through *in situ* growth from the authigenic alteration of precursor and early-diagenetic minerals, which interact with pore fluids during burial (Hillier 1994; Aagaard et al. 2000; Worden and Morad 2003; Ajdukiewicz and Larese 2012). The clay-coat coverage (i.e., the fraction of the sand-grain surface covered by clay minerals), as well as the mineralogy of the clay coat, have been reported to be the dominant controls on the ability of authigenic clay coats to inhibit quartz cementation (Billault et al. 2003; Lander et al. 2008;

Ajdukiewicz and Larese 2012). The availability of iron is essential to the creation of porosity-preserving Fe-bearing authigenic chlorite during burial diagenesis. In sediment, if iron is preferentially locked up as either pyrite or siderite, then it will be unavailable to create Fe-silicate minerals such as chlorite during subsequent diagenesis. Pyrite and siderite grow much more quickly than the Fe-silicate clay minerals (such as chlorite), so that, if there is competition at any one time, then pyrite or siderite will preferentially grow at the expense of authigenic chlorite (Worden and Morad 2003).

Clay minerals in sandstones (including the minerals in clay coats) are probably not a result of the mass influx of materials into sandstones during burial diagenesis, since many of the main components of clay minerals (for chlorite: Fe, Mg, Al, and Si oxides) are effectively water-insoluble, even during the long time scale over which burial diagenesis occurs (Worden and Morad 2003). As a result, it has been concluded that the clay minerals present in sandstones (both pore-filling and grain-coating) are controlled by the primary depositional composition, i.e., the mineralogy of precursor components in the initial sediment (Worden and Morad 2003). As a result, the study of distribution patterns of detrital minerals (clay and framework

grains) in modern sedimentary settings will facilitate prediction of the spatial distribution of authigenic clay minerals in ancient and deeply buried sandstones, such as chlorite.

The fundamental motivation for this study was to establish how detrital clay coats and clay minerals (chlorite, illite, kaolinite, and smectite) are distributed in the near-surface (one meter cores;  $n = 23$ ) of a modern estuarine setting (Ravenglass Estuary, UK; Fig. 1), on a scale similar to many oil and gas fields. This study provides the first integrated near-surface study, which compares the relationship between lithofacies, Fe-sulfides, and detrital clay minerals and clay coats in estuarine sediments, and can be used, by analogy, to better predict petroleum reservoir quality.

It has been reported that distribution patterns of detrital clay coats in surface sediment (here defined as sediment from  $< 2$  cm depth) of the Ravenglass Estuary are controlled by the physical attachment of clay-size material to sand-grain surfaces by adhesive extracellular polymeric substances (biofilms) secreted by diatoms during locomotion (Jones 2017; Wooldridge et al. 2017a; Wooldridge et al. 2018). Experiments showed that detrital clay coats can develop through the direct ingestion and excretion of sediment by *Arenicola marina* (lugworms), by creating a sticky mucus membrane that adheres fine-grained sediment to the surface of sand grains (Needham et al. 2005; Worden et al. 2006). In contrast, Wooldridge et al. (2017b) showed that in surface sediment ( $< 2$  cm) in the Ravenglass Estuary, there is no spatial correlation between the population density of *Arenicola marina* and the extent of detrital-clay-coat coverage. However, as acknowledged by Wooldridge et al. (2017b), it remains unknown whether sediment bioturbation by *Arenicola marina*, or other estuarine macro fauna, might form clay coats at sediment depths greater than 2 cm. Furthermore, clay coats have been suggested to originate from the postdepositional mechanical infiltration of clay-laden waters through the pore spaces of sediments in modern sediments and in ancient sandstones (Matlack et al. 1989; Moraes and De Ros 1990; Wilson 1992; Buurman et al. 1998). A primary aim of this study was therefore to establish whether surface ( $< 2$  cm) distribution patterns of detrital-clay coats in the Ravenglass Estuary (Wooldridge et al. 2017a; Wooldridge et al. 2017b) are transferred to the immediate near-surface (here defined as depths  $< 1$  m), or whether they are overprinted by postdepositional processes (e.g., bioturbation or mechanical infiltration).

A combination of climate (i.e., intensity of chemical and mechanical weathering), relief (i.e., topographic elevation), and provenance (i.e., sediment supplied) has been proposed to control the type and abundance of clay minerals (clay-mineral assemblage) found in modern oceanic and marginal-marine settings (Eberl et al. 1984; Chamley 1989; McKinley et al. 2003; Rateev et al. 2008). It has been suggested that clay-mineral distribution patterns in marginal-marine sedimentary systems might be controlled by: the landward displacement of marine sediment (Postma 1967; Meade 1969; Hathaway 1972; Chamley 1989), differential settling due to salinity or clay-mineral stability (Whitehouse et al. 1960; Edzwald and O'Mella 1975), the physical sorting of clay minerals by size (Gibbs 1977), local hydrodynamics (Feuillet and Fleischer 1980), provenance (Biddle and Miles 1972; Hathaway 1972; Feuillet and Fleischer 1980; Rudert and Müller 1981), mechanical infiltration (Matlack et al. 1989), and both early physicochemical (Grim and Johns 1954; Griffin and Ingram 1955; Powers 1957; Nelson 1960) and biologically mediated diagenesis via sediment bioturbation (McIlroy et al. 2003; Needham et al. 2004; Needham et al. 2005; Needham et al. 2006; Worden et al. 2006).

In summary, a detailed shallow-core study of the Ravenglass Estuary, UK has been designed to address the following specific research questions, in order to provide a modern analogue for the prediction of distribution patterns of clay minerals, clay coats, and Fe-sulfides in marginal-marine sandstone reservoirs.

- How are detrital clay coats distributed in near-surface ( $< 1$  m) estuarine sediment? How do near-surface detrital-clay-coat distribution patterns compare to surface ( $< 2$  cm) detrital-clay-coat distribution patterns

reported by Wooldridge et al. (2017b)? What are the fundamental controls on detrital-clay-coat distribution patterns in near-surface sediment?

- Which clay minerals are found in near-surface sediment of the Ravenglass Estuary? How are clay minerals distributed? What controls clay-mineral distribution patterns?
- Which Fe-sulfides are found in near-surface sediment of the Ravenglass Estuary? How are Fe-sulfides distributed? What controls clay Fe-sulfide distribution patterns?
- Can distribution patterns of precursor detrital clay coats, clay minerals and/or Fe-sulfides be predicted as a function of lithofacies in the Ravenglass Estuary? In ancient and deeply buried estuarine sandstones, based on results of this study, which depositional environments are likely to have the best reservoir quality?

#### STUDY AREA: RAVENGLASS ESTUARY

##### *Geomorphology and Estuarine Hydrodynamics*

The Ravenglass Estuary is located in northwest England on the west coast of Cumbria, and encompasses the tidal reaches of the westward-flowing Rivers Irt, Mite, and Esk (Fig. 1A–D). The inner estuary and central basin are sheltered from wave action by two coastal spits (Drigg and Eskmeals), but are subject to strong tidal currents owing to a macrotidal regime ( $> 7$  m tidal range). The Ravenglass Estuary is here classified as a “dual-funneled” and mixed-energy system. The Ravenglass Estuary is shallow (Fig. 1B), and occupies an area of 5.6 km<sup>2</sup> of which approximately 86% is intertidal (Bousher 1999; Lloyd et al. 2013; Wooldridge et al. 2017b). The shallow bathymetry causes frictional effects that promote strong tidal asymmetry, resulting in prolonged outward ebb tidal flow in comparison to the inward tidal flow (Kelly et al. 1991). The rivers flowing into the estuary have average flow rates of 0.4 m<sup>3</sup>s<sup>-1</sup> for the Mite, 3.4 m<sup>3</sup>s<sup>-1</sup> for the Irt, and 4.2 m<sup>3</sup>s<sup>-1</sup> for the Esk (Bousher 1999). The short length of the estuary (due to geologically mediated topographic constraints) has been reported to cause quick ebb drainage, meaning that the maximum discharge measured for the lower-Esk arm of the estuary during the ebb tidal flow (4.99 m<sup>3</sup> s<sup>-1</sup>) is only slightly lower than flood tidal flow (5.41 m<sup>3</sup> s<sup>-1</sup>) (Kelly et al. 1991). Anthropogenic impact on the estuary is here considered to be minor, with exception of sheltering of the inner Mite and increased salt-marsh development as a consequence of the railway viaduct construction (Fig. 1A) (Carr and Blackley 1986).

##### *Geological Setting, Hinterland Bedrock, and Quaternary Drift*

The Ravenglass Estuary is fed by two river catchments, the northern River Irt and River Mite, and the southern River Esk. The River Irt and River Mite predominantly drain Ordovician Borrowdale Volcanic Group andesites and Triassic Sherwood Sandstone Group sedimentary rocks (Fig. 1C). The River Esk drains an area dominated by the Devonian Eskdale Granite. The weakly metamorphosed, fine-grained sedimentary rocks of the Skiddaw Group (Merritt and Auton 2000) has marginal exposure at Muncaster Fell (Fig. 1C). The Borrowdale Volcanic Group is dominated by subduction-related, K-rich, calc-alkaline andesite, and was subject to regional, sub-greenschist-facies metamorphism at about 395 Ma during the Caledonian Orogeny (Quirke et al. 2015). Chlorite is abundant in the Borrowdale Volcanic Group and has been reported to occur as pseudomorphs after pyroxene (Quirke et al. 2015). The Lower Triassic Sherwood Sandstone Group (locally known as the St Bees Sandstone) is composed predominantly of fluvial sandstones (Quirke et al. 2015). The northern part of the Eskdale Granite is a coarse-grained granite, and the southern part is granodioritic (Young et al. 1986). Chloritization of mafic silicates and plagioclase alteration are widespread in both Eskdale granite types (Moseley 1978; Young et al. 1986; Quirke et al. 2015).



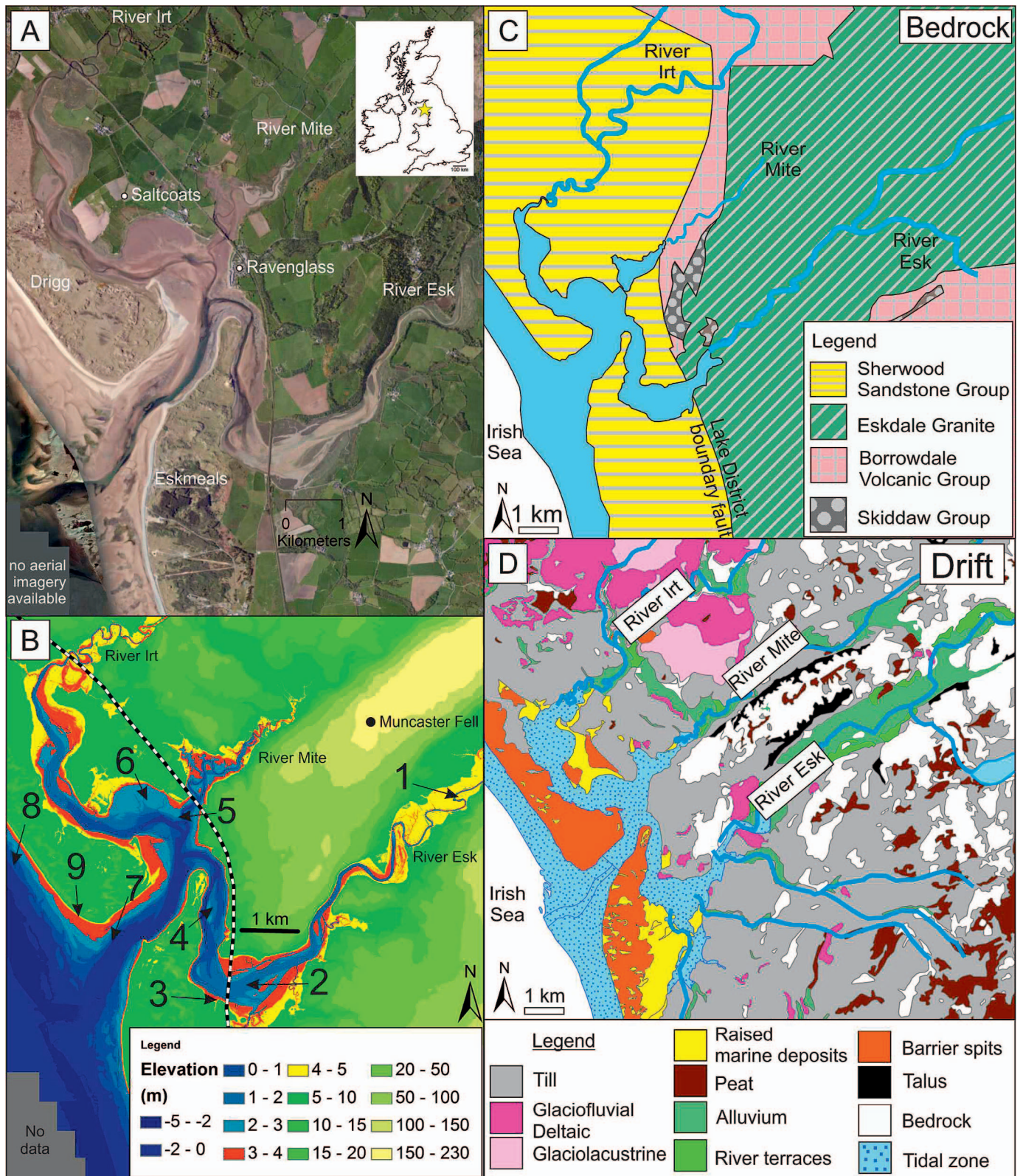


Fig. 1.—Study location, Ravenglass Estuary, UK. **A)** Aerial image of the Ravenglass Estuary, UK. **B)** Estuarine bathymetry and hinterland elevation (m OD) derived from Lidar Imagery collected by the UK Environmental Agency (UK Environmental Agency 2015). The position of nine core regions highlight the location of core samples (n = 23). Shades of blue highlight intertidal regions, red-colored areas highlight the extent of salt-marsh and backshore deposits, and yellow-colored areas highlight the extent of fluvial floodplains. **C)** Bedrock geology and **D)** Quaternary drift deposits.



TABLE 1.—*Bioturbation-index classification scheme, after Taylor and Goldring (1993).*

BI	Classification of Bioturbation Index (BI).
0	No bioturbation
1	Sparse bioturbation, bedding distinct, few discrete traces and/or escape structures
2	Low bioturbation, bedding distinct, low trace density, escape structures often common
3	Moderate bioturbation, bedding boundaries sharp, traces discrete, overlap rare
4	High bioturbation, bedding boundaries indistinct, high trace density with overlap common
5	Intense bioturbation, bedding completely disturbed (just visible), limited reworking, later burrows discrete
6	Complete bioturbation, sediment reworking due to repeated overprinting.

The northern part of the UK (including Cumbria) is presently undergoing limited isostatic recovery following the last glacial maximum (Bousher 1999) which occurred in the late Devensian at about 28 to 13 ka (Moseley 1978; McDougall 2001). Glacioisostatic rebound following deglaciation, together with glacioeustatic sea-level change, led to fluctuations in relative sea level during the Holocene, which resulted in the deposition of a suite of tills and glaciofluvial and glaciolacustrine deposits (Fig. 1D). Much of the glacial deposit has been removed from the land surface following the last glaciations (Merritt and Auton 2000). Drift deposits are locally known as the Seascale Glacigenic Formation (the Ravenglass Till member being the dominant unit in the Ravenglass area) and the overlying Gosforth Glacigenic Formation (Merritt and Auton 2000; Lloyd et al. 2013). Estuarine sediments are therefore underlain by glacial till which is exposed as knolls throughout the estuary. The postglacial estuarine sediments, the subject of this study, have a maximum thickness of ~ 10 to 15 meters in this area (Bousher 1999). Quaternary sediments contain distinctive clasts of the underlying bedrock, which allows detailed lithostratigraphical division as well as revealing complex ice-movement patterns (Merritt and Auton 2000).

#### SAMPLES AND METHODS

##### *Field Mapping and Core Collection*

Detailed ground surveys, aided by aerial imagery (Fig. 1A) and LIDAR survey (Fig. 1B) (UK Environmental Agency 2015) were used to define a suite of estuarine environments. Tidal flats were differentiated based on sand abundance, following the tidal-flat classification scheme proposed by Brockamp and Zuther (2004) whereby a sand flat is > 90% sandgrade material, a mixed flat has 50 to 90% sand grade material, and a mud flat has 15 to 50% sand grade material. Sand abundance was determined for sediment samples using a Beckman Coulter Laser Particle Size Analysis (LPSA) in unison with GRADISTAT (Blott and Pye 2001).

Twenty-three cores, covering nine regions (labeled 1 to 9 in Fig. 1B), were collected, along predefined transects, in order to capture surface-sediment heterogeneity. Cores were collected with negligible sample disturbance using a jackhammer-driven window sampler following the method detailed by Dowey et al. (2017). Each core was retrieved in a polythene liner to avoid oxidation and sample degradation, and protected in a rigid plastic tube.

##### *Core Preparation and Description*

Sediment cores were dissected and photographed, wet and dry, to capture redox boundaries, ichnofabrics (bioturbation traces), and key

sedimentary structures in the laboratory. Core samples collected for X-ray diffraction analysis were extracted and placed in an air-tight, screw-top plastic jar, stored in the dark, and refrigerated (at ~ 2 °C) to avoid degradation before analysis. Sediment samples, used to determine detrital-clay-coat coverage, were collected following the same procedure outlined by Wooldridge et al. (2017b).

Sediment grain-size was measured in the laboratory using a hand lens and grain-size card every 5 cm in relatively homogeneous facies, and at a sub-centimeter scale where necessary, e.g., in very thin-bedded sediment (< 3 cm). In this study, the Campbell (1967) classification to assign bed thickness was used. Wavy flaser bedding and wavy-bedded heterolithics have been defined following Reineck and Wunderlich (1968). Bioturbation Index (BI) was recorded using the classification scheme proposed by Taylor and Goldring (1993) (Table 1) to test the strength of the relationship between bioturbation intensity, mineralogy, and extent of detrital-clay-coat coverage.

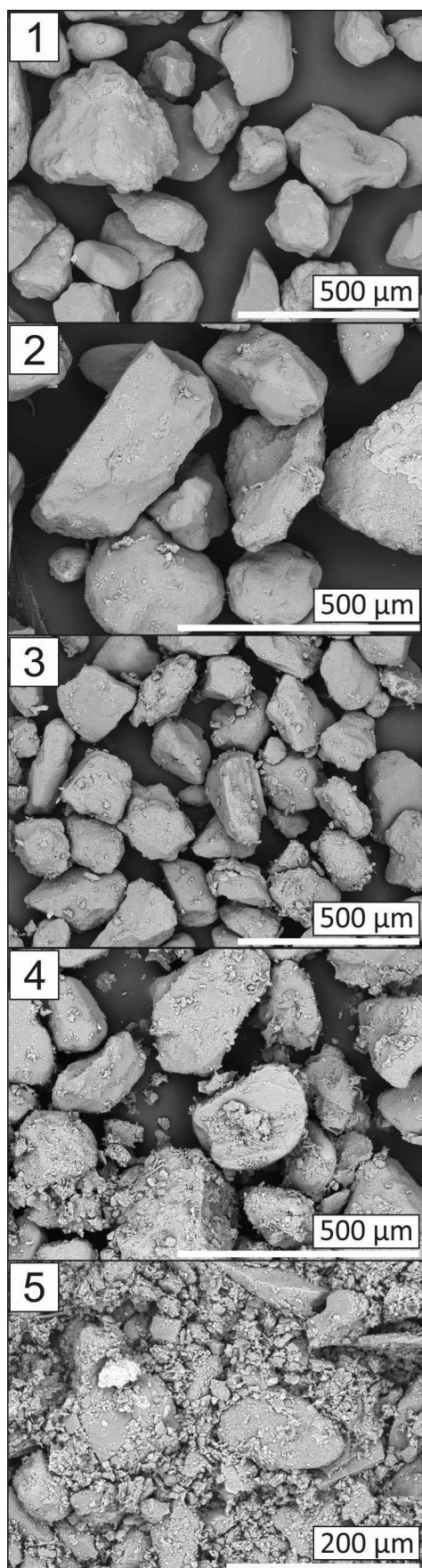
##### *Qualitative Analysis of Clay-Coat Coverage*

To achieve a direct comparison between detrital clay-coat-coverage in surface sediment (< 2 cm) and near-surface (< 1 m) sediment, detrital clay-coat-coverage was determined qualitatively following the methodology and classification scheme proposed by Wooldridge et al. (2017b) (Fig. 2). A qualitative estimation of clay-coat coverage on individual sand grains (five principal classes; Fig. 2) was achieved by analyzing 200 sand grains (per grain-mount sample), imaged using scanning electron microscopy (SEM). The following bin classes, defined by Wooldridge et al. (2017b), were used: (Class 1) complete absence of clay coats; (Class 2) less than half of the grains have a small (~ 1 to 5%) surface area of attached clay coats; (Class 3) every grain exhibits at least ~ 5 to 15% clay-coat coverage; (Class 4) extensive (~ 15 to 30%) clay-coat coverage on the majority of grains; (Class 5) greater than 30% surface area covered by clay coats on every grain (Fig. 2). Environmental SEM analysis was undertaken to image hydrated sediment samples for the presence of diatoms in life position (not dried out). The QEMSCAN® system, consisting of a scanning electron microscope (SEM) coupled with energy-dispersive spectrometers (EDS), was used to establish the major mineralogical components of detrital clay coats. Data were collected with a step size of 2 µm to ensure both the fine fraction (< 2 µm) and silt and sand fraction (> 2 µm) was analyzed.

##### *Clay-Mineral Separation, Identification, and Quantification*

The clay fraction (< 2 µm) of dried and weighed representative core sub-samples and Quaternary glaciogenic drift deposits (sourced from cliff sections in the inner Esk) were physically separated (isolated from the silt and sand fraction) before XRD analysis. This was performed using an ultrasonic bath to disaggregate sediment, followed by gravity settling to separate out the sand and silt size fractions, and then centrifuge settling at 5,000 rpm for 10 minutes to collect the clay size fraction. The separated clay fraction was then dried at 60 °C for 24 hours and weighed to calculate the percentage of clay-size material. The mineralogy of the clay fraction was determined using a PANalytical X'Pert Pro MPD X-ray Diffractometer (Fig. 3). Samples were glycolated for 24 hours and re-scanned over a range of 3.9 to 13.0° 2θ to test for the presence of expandable clay minerals (i.e., smectite) following the methodology outlined by Moore and Reynolds (1997). It was decided to perform XRD analyses on randomly oriented powders, as opposed to oriented mounts, because the precise (repeatable) quantification of all minerals, not just clay minerals, was the most important goal of this study. The mineralogy of the clay fraction was determined by comparing acquired diffractograms with those in the International Centre for Diffraction Data Powder Diffraction File-2008, and supplementary information from Moore and Reynolds (1997). The minerals were then quantified using the relative intensity ratio (RIR)





method proposed by (Chung 1974a) and (Chung 1974b) using Panalytical HighScore Plus software. Although the reliability of the RIR method can be affected by the crystallinity and chemistry of a given mineral, the results from this quantification method have been reported to be highly accurate (Hillier 2000, 2003). Significant emphasis was here placed on consistent and precise XRD preparation, analysis, and quantification methods, employed by a single operator, at all stages of sample preparation and analysis, to ensure the highest possible degree of inter-sample comparability.

The term *illite* in this paper refers to the clay-size mica-like minerals (10 Å non-expandable clay) typically found in argillaceous rocks (Grim et al. 1937), also termed *illitic material* (Moore and Reynolds 1997). Furthermore, in an attempt to differentiate illite types in the Ravenglass estuarine sediment, based on composition and crystallinity, we have calculated the Esquevin Index and illite crystallinity for each sample (Fig. 3).

The Esquevin Index has been calculated to differentiate Al-rich from Fe-Mg-rich illite. The Esquevin Index is calculated by analyzing the ratio between the (002) and (001) peak heights (Esquevin 1969), on X-ray diffractograms, i.e., the ratio between the intensity of the 5 Å and 10 Å peaks (Fig. 3). The following classification boundaries are used in this study, after Esquevin (1969): biotite, < 0.15; biotite + muscovite, 0.15 to 0.3; phengite, 0.3 to 0.4; muscovite, > 0.4. Thus, high Esquevin Indices indicate Al-rich illite, whereas low Esquevin Index values represent relatively Fe-Mg-rich illite. Low Esquevin Indices are characteristic of physically eroded, unweathered rocks (Chamley 1989). High Esquevin Indices correspond to chemically weathered rocks that have lost divalent cations (Fe and Mg) from the octahedral sites (Chamley 1989).

The full width at half-maximum (FWHM) of the 10 Å (001) illite peak was measured on X-ray diffractograms in order to establish illite crystallinity index ( $2^\circ \theta$ ), also known as the *Kübler Index* (Kübler 1964). Poorly crystalline illite is reflected by broad basal reflections (high FWHM values), associated with highly degraded, low-growth-temperature, low-structural-order illite (Kübler 1964; Chamley 1989). Highly crystalline illite is reflected by narrow basal reflections (low FWHM values), associated with relatively unaltered, high-growth-temperature, high-structural-order illite (Kübler 1964; Chamley 1989). The following boundaries are used, after Kübler (1964): epizone (highest temperature): < 0.25; anchizone: 0.25 to 0.42; diagenesis (lowest temperature): > 0.42. To assess relative clay-mineral abundance, clay-mineral indices were derived as follows: relative abundances of chlorite: (chlorite/(chlorite + illite + kaolinite + smectite)), kaolinite: (kaolinite/(chlorite + illite + kaolinite + smectite)), illite: (illite/(chlorite + illite + kaolinite + smectite)) and smectite: (smectite/(chlorite + illite + kaolinite + smectite)).

The mineralogy of discrete grain-size fractions from a single disaggregated sample from the Saltcoats mudflat in the central zone of the Ravenglass Estuary was achieved using a combination of sieving and gravity settling (as above) followed by X-ray diffraction analysis of each grain-size fraction. Grain-size classes included: < 0.2 μm (fine clay); 0.2 μm to 2 μm (coarse clay); 2 μm to 32 μm (fine silt); 32 μm to 62 μm (coarse silt); 62 μm to 125 μm (very fine sand); and 125 μm to 250 μm (fine sand).

Fig. 2.—Secondary electron (SE) images categorizing the extent of detrital-clay-coat coverage observed in near-surface (< 1 m) sediment samples in the Ravenglass Estuary, UK. The detrital-clay-coat classification approach has been adopted from Woodriddle et al. (2017b). (Class 1) Complete absence of clay coats. (Class 2) Less than half of the grains have a small (~ 1–5%) surface area of attached clay coats. (Class 3) Every grain exhibits at least ~ 5–15% clay-coat coverage. (Class 4) Extensive (~ 15–30%) clay-coat coverage on the majority of grains. (Class 5) Greater than 30% surface area covered by clay coats on every grain.

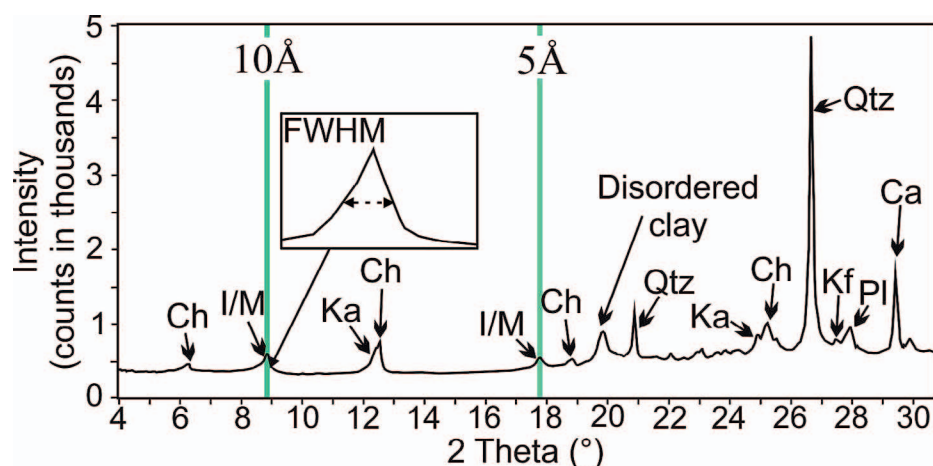


FIG. 3.—Example of an X-ray diffractogram used to quantify clay-mineral abundance. The Esquevin Index is derived by comparing the relative peak heights of the 5 Å and 10 Å illite peaks (highlighted by a green line). Illite crystallinity is measured on the 10 Å illite peak, using the full width at half maximum (FWHM).

### Statistical Analysis

Statistical analysis was performed to test whether lithofacies, sediment depth (proxy for mechanical infiltration), and bioturbation index (intensity) might explain distribution patterns of clay minerals, pyrite, and/or detrital clay coats in the Ravenglass Estuary. All statistical analyses were performed in R statistical software (R Core Team 2016), using the following symbols to highlight statistical significance: marginally significant (+) when  $p < 0.1$ ; significant (\*) when  $p < 0.05$ ; very significant (\*\*) when  $p < 0.01$ ; and extremely significant (\*\*\*) when  $p < 0.001$ . Outliers (open circles) in box and whisker plots are defined as an observation that is numerically distant from the rest of the data (i.e., a value that is 1.5 times the interquartile range below the lower quartile and above the upper quartile). Note that statistical analyses were not performed on any lithofacies which had a sample number less than 3.

### Clay Coats: Lithofacies, Bioturbation Intensity, and Core Depth

A Kruskal-Wallis H test was used to test whether there is a statistically significant difference in detrital-clay-coat coverage as a function of estuarine lithofacies. Following the Kruskal-Wallis H test, a post-hoc Dunn test was employed to highlight where the identified significant differences occurred in detrital-clay-coat coverage between individual facies. The Benjamini-Hochberg method (False Discovery Rate) (Benjamini and Hochberg 1995) was applied to correct the  $p$ -values after performing multiple comparisons.

Pearson's correlation coefficients were calculated to describe the strength of the relationship between clay-fraction abundance and core depth, to assess whether there is any evidence for a postdepositional increase in clay content, which might be due to mechanical infiltration. In order to determine whether mechanical infiltration might have led to the post-depositional formation of clay coats, Spearman's correlation coefficients were calculated to describe the strength of the relationship between clay-coat coverage and core depth. To assess whether the act of sediment bioturbation might form clay coats, Spearman's correlation coefficients were calculated to test the strength of the relationship between Bioturbation Index (BI) and extent of clay coat coverage.

### Mineralogy: Lithofacies, Bioturbation Intensity, and Core Depth

An Analysis of Variance (ANOVA) test was used to test whether there is a statistically significant difference in clay-mineral indices (chlorite, illite, kaolinite, and smectite) and pyrite abundance, as a function of estuarine lithofacies. Following ANOVA, a post-hoc Tukey's honestly significant difference (HSD) test was employed to highlight where the identified

significant differences in relative abundance of clay minerals and/or pyrite between individual facies could be found.

The strength of the relationship between depth and clay-mineral indices was calculated using Pearson's correlation coefficients to test whether vertical mechanical infiltration might have led to the stratification of clay minerals. Pearson's correlation coefficients were calculated to test the strength of the relationship between depth and pyrite abundance in order to determine whether pyrite formation is controlled principally by sediment depth (i.e., increasing anoxic conditions with an increase in sediment depth). It is acknowledged that redox-boundary depth is also dependent on other variables, such as sediment properties (e.g., grain size and sorting) and bioturbation type and intensity. To establish whether bioturbation might have led to the early-diagenetic alteration and/or formation of new clay minerals, Spearman's correlation coefficients were used to test the strength of the relationship between Bioturbation Index (BI) and clay-mineral indices.

## RESULTS

The surface characterization of the Ravenglass Estuary, as well as sedimentary logs, a detailed facies scheme, mineralogical analyses (clay mineral indices, pyrite abundance, Esquevin index, and illite crystallinity), and data on clay-coat distribution from twenty-three one-meter cores is here presented.

### Surface Depositional Environments and Facies Associations

The eleven discrete depositional environments in the Ravenglass Estuary are presented in Figure 4. The eight depositional environments that were cored (Figs. 5–11) are characterized by eight sedimentary facies associations (FAs; Table 2) in the near-surface, namely: floodplain (FA 1), salt marsh (FA 2), mud flat (FA 3), mixed-flat and thin-bedded sediments (FA 4), low-amplitude dunes and tidal bars (FA 5), glacial armored surface (FA 6), tidal inlet and foreshore (FA 7), and coastal spits (FA 8; Fig. 4). The descriptive characteristics (texture, sedimentary structures, and ichnofabrics) for each lithofacies, which can be used to characterize specific depositional environments, are summarized in Table 2. The abundance (%) of each facies in each core is summarized in Figure 12.

### Detrital-Clay-Coat Coverage: Lithofacies, Bioturbation Intensity, and Core Depth

Detrital-clay-coat coverage, measured for each core, is presented next to individual schematic sedimentary logs in Figures 5 to 11. Micron-scale (2  $\mu\text{m}$ ) SEM and SEM-EDS (QEMSCAN®) analysis reveal that the chief component of detrital clay coats in the Ravenglass Estuary are clay minerals



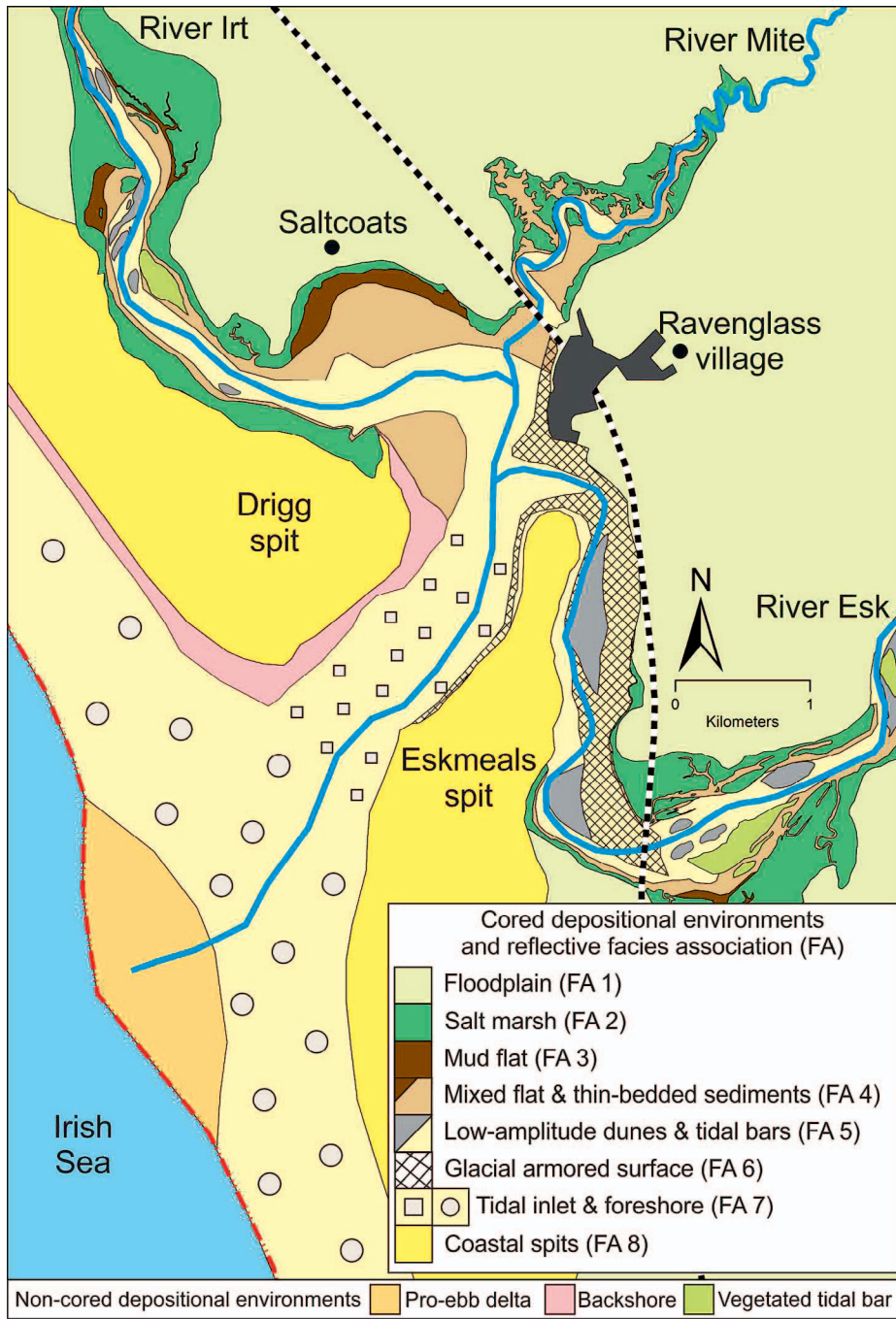


FIG. 4.—Type and distribution of cored estuarine depositional environments and corresponding facies associations (FAs) in the Ravenglass Estuary.

(Fig. 13A) and, if present, pyrite (Fig. 13B). The abundance (average and standard deviation) of clay fraction (< 2 μm) in each lithofacies is summarized in Table 3. There is a strong, positive correlation between clay-fraction abundance and detrital-clay-coat coverage ( $r = 0.92, p < 0.001$ ). Average clay fraction for each lithofacies ranges from 0.1% to 22.6%, with a weighted estuarine clay fraction average of 5.9% (Table 3). The range, upper and lower quartile, and median of clay-fraction abundance (%) for each lithofacies, and for each core, are presented in Figure 14.

The variability of clay-coat coverage (relative abundance of classes 1 to 5) for each lithofacies is summarized in Figure 15. Kruskal-Wallis H test results show there is a statistical difference ( $p < 0.05$ ) in the extent of detrital-clay-coat coverage between lithofacies. Post-hoc Dunn test results

(Table 4) reveal between which lithofacies there are statistical differences in detrital-clay-coat coverage.

There is a strong, positive correlation between detrital-clay-coat coverage and bioturbation index ( $r = 0.84, p < 0.001$ ). Environmental scanning electron microscopy (ESEM) of hydrated near-surface sediments show an abundance of epipellic diatoms, which appear to have secreted extracellular polymeric substances (EPS) and attaching clay particles to the surface of sand grains (Fig. 13C). Secondary Electron microscopy (SE) of dried sediment reveals an abundance of epipellic diatoms, typically imbedded in clay coats (Fig. 13D).

Pearson's correlation coefficient test results reveal that there is no consistent relationship between depth below the sediment surface and the

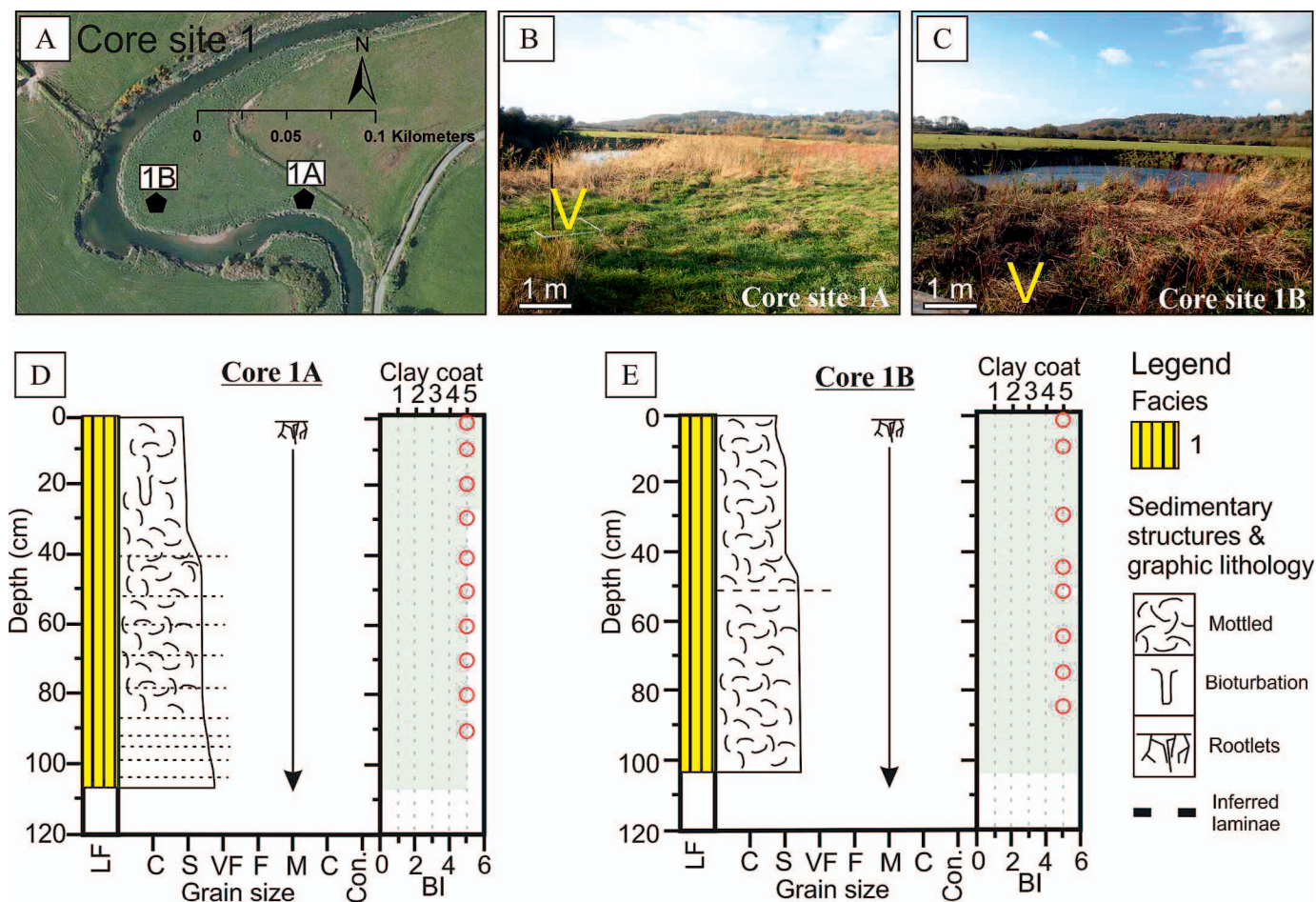


FIG. 5.—Core locations and schematic sedimentary logs of River Esk floodplain deposits (FA 1; cores 1A and 1B). **A)** Map of site for cores 1A and 1B (see Fig. 1B for location). **B)** Photograph of core site 1A (yellow “V” symbols represent the location of where individual cores were collected). **C)** Photograph of core site 1B. **D)** Log for core 1A with detrital clay coat coverage (red circles) and bioturbation index (BI) (grayed area) presented next to each schematic sedimentary log. **E)** Log for core 1B including detrital-clay-coat coverage and bioturbation index. Refer to Table 2 for explanation of facies codes and Table 2 for the classification of clay-coat coverage.

abundance of clay fraction (Table 5). Spearman’s correlation coefficient test results also reveal that there is no consistent relationship between depth below the sediment surface and the extent of detrital-clay-coat coverage (Table 5).

#### Mineralogy: Lithofacies, Bioturbation Intensity, and Core Depth

The relative abundance of the three dominant clay minerals (illite, chlorite, and kaolinite) as a function of facies association (FAs; Table 2) is shown in Figure 16. All FAs are dominated by illite (> 50%). Illite is most abundant in FAs 2 to 4 (> 60%). FAs 1, 7, and 8 are relatively enriched in chlorite (> 20%). Kaolinite is relatively ubiquitous and is typically present in abundances ~ 20 to 25% (Fig. 16).

The relative abundance of chlorite, kaolinite, illite, and smectite, as well as Esquevin Indices, illite crystallinity, and the abundance of pyrite in each lithofacies are summarized in Table 3. The range, upper and lower quartile, and median for each specific clay-mineral index as a function of lithofacies are presented in Figure 17. The range, upper and lower quartile, and median for Esquevin index, illite crystallinity, and quantity of pyrite as a function of lithofacies are presented in Figure 18.

Analysis of Variance (ANOVA) test results reveal chlorite, illite, kaolinite, and smectite abundance is significantly different ( $p < 0.001$ )

between lithofacies. The multi-comparison, post-hoc Tukey HSD test results reveal between which individual lithofacies there are statistical differences (Table 6).

The range, upper and lower quartile, and median of clay-mineral and Esquevin indices, as well as illite crystallinity and pyrite abundance as a function of core position, are represented in Figures 19 and 20. Pearson’s test results show that there is no consistent relationship between core depth and the relative abundance of chlorite, illite, and kaolinite (Table 5). Pyrite abundance typically increases with depth in central-basin estuarine cores (cores 6A, 6B, and 6C; Fig. 1B); Pearson’s correlation coefficients range from 0.74 to 0.91 ( $p < 0.001$ ) (Table 5).

The relationship between bioturbation index and the relative abundance of chlorite, illite, and kaolinite is presented in Figure 21. Chlorite typically decreases with an increase in bioturbation intensity ( $r = -0.62$ ,  $p < 0.001$ ), illite abundance broadly increases with an increase in bioturbation intensity ( $r = 0.49$ ,  $p < 0.001$ ), and kaolinite abundance shows little relationship with bioturbation intensity ( $r = -0.18$ ,  $p < 0.05$ ).

#### Clay-Mineral Abundance as a Function of Grain-Size Fraction

The relative abundance of clay minerals (chlorite, illite, kaolinite, and smectite) for each grain-size separate from a single disaggregated sediment



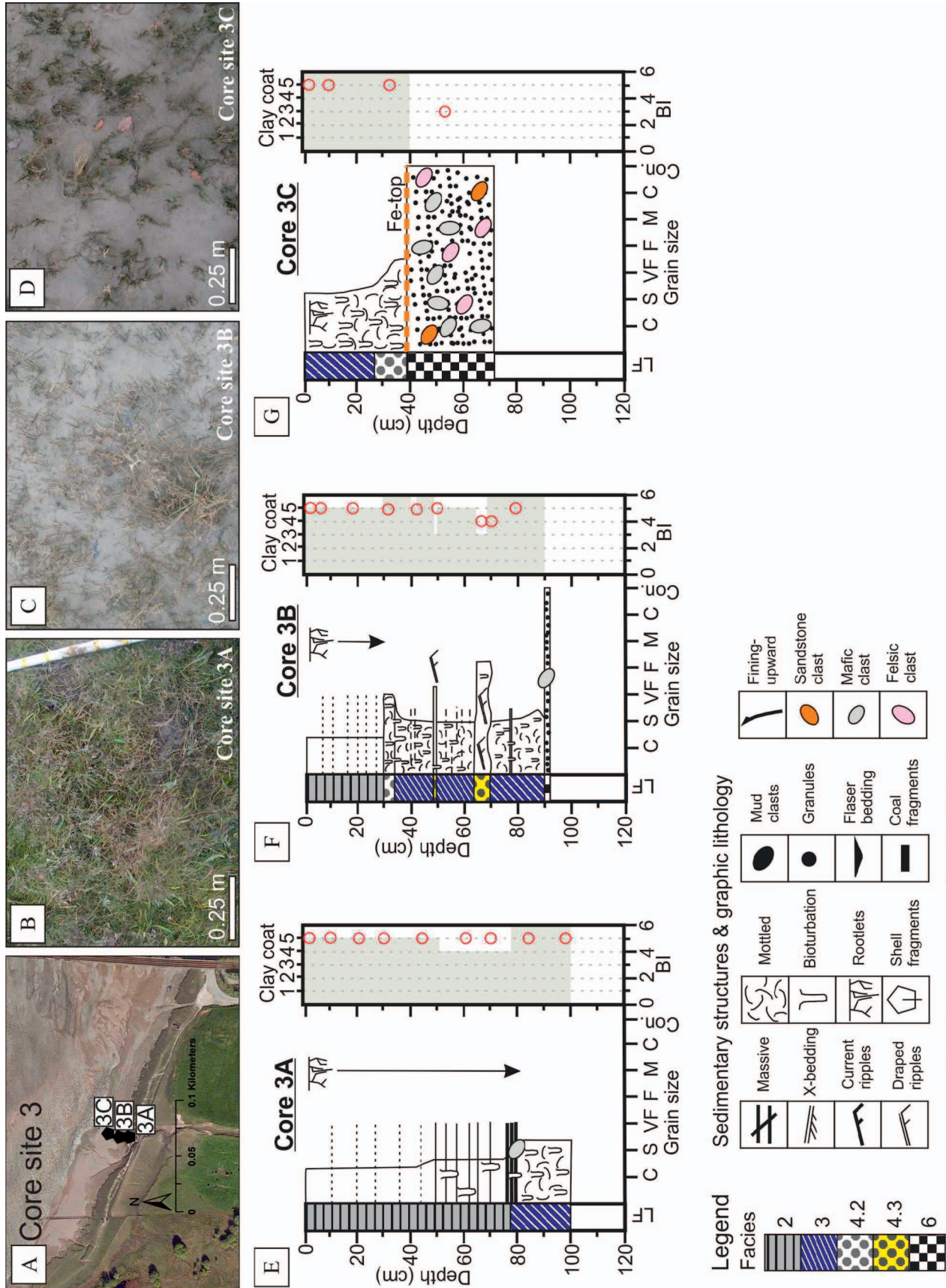


Fig. 6.—Core locations and schematic sedimentary logs of inner River Esk salt-marsh deposits (FA 2); well-vegetated upper-tier salt marsh (core 3A), moderately vegetated middle-tier salt marsh (core 3B), and moderately to sparsely vegetated lower-tier salt marsh (core 3C). **A**) Map of site for cores 3A to 3C (see Fig. 1B for location). **B**) Photograph of core site 3A. **C**) Photograph of core site 3B. **D**) Photograph of core site 3C. **E**) Log for core 3A with detrital-clay-coat coverage (red circles) and bioturbation index (BI) (grayed area) presented next to each schematic sedimentary log. **F**) Log for core 3B including detrital-clay-coat coverage and bioturbation index. **G**) Log for core 3C including detrital-clay-coat coverage (red circles) and bioturbation index (BI) (grayed area) are presented next to each schematic sedimentary log. Refer to Table 2 for explanation of facies codes and Figure 2 for the classification of clay coat coverage.



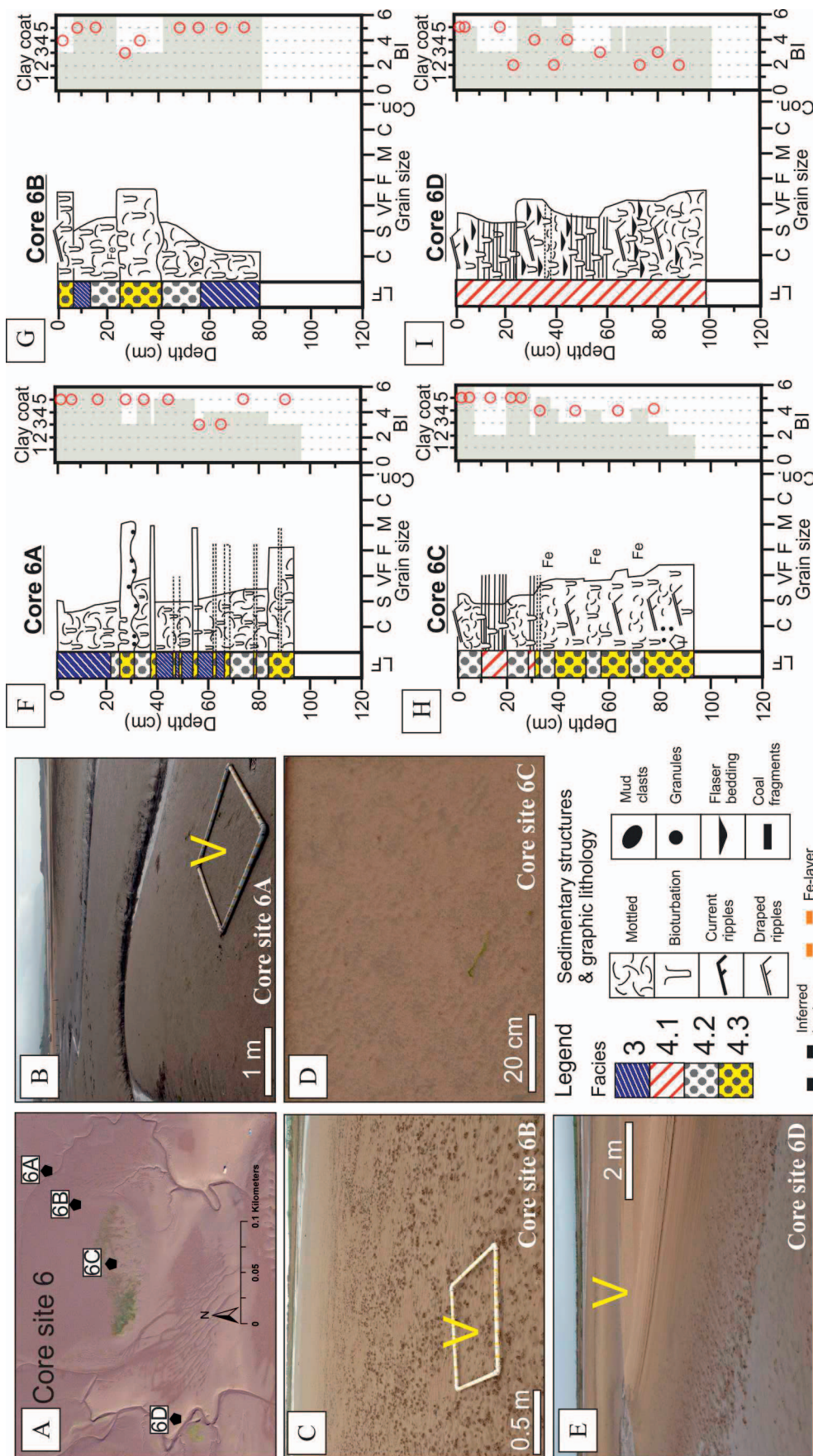


FIG. 7.—Core locations and schematic sedimentary logs of mud flat and mixed flat with incursions of thin-bedded sediments, as well as heterolithic tidal-creek point-bar deposits (FAs 3 and 4). **A**) Map of site for cores 6A to 6D (see Fig. 1B for location). **B**) Photograph of core site 6A. **C**) Photograph of core site 6B. **D**) Photograph of core site 6C. **E**) Photograph of core site 6D. **F**) Log for core 6A with detrital-clay-coat coverage (red circles) and bioturbation index (BI) (grayed area) presented next to each schematic sedimentary log. **G**) Log of core 6B, including detrital-clay-coat coverage and bioturbation index. **H**) Log of core 6C, including detrital-clay-coat coverage and bioturbation index. **I**) Log of core 6D including detrital-clay-coat coverage and bioturbation index. Refer to Table 2 for explanation of facies codes and Figure 2 for the classification of clay-coat coverage.



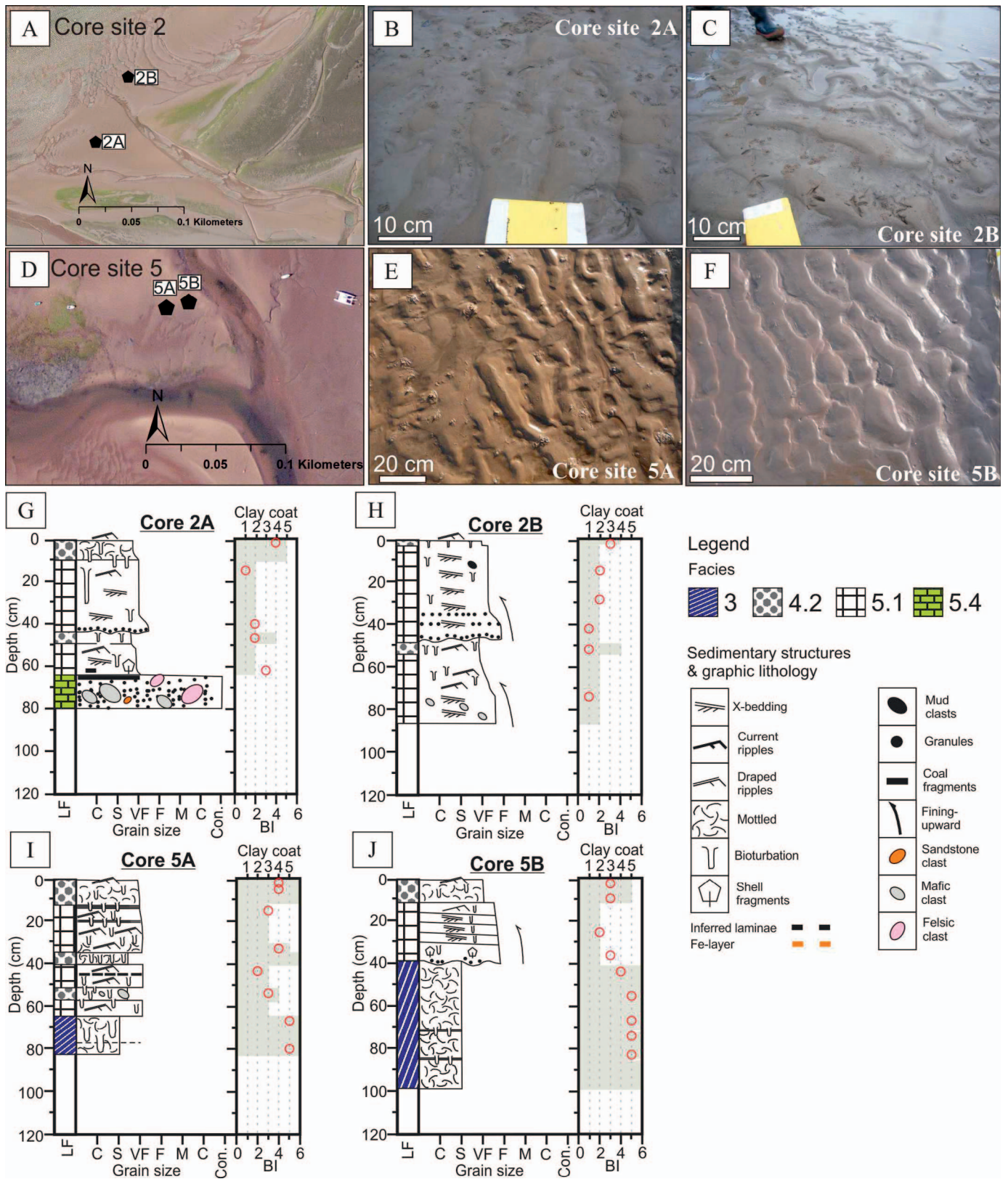


FIG. 8.—Core locations and schematic sedimentary logs of low-amplitude dunes (FA 5) that fine upward into bioturbated (primarily *Arenicola marina*; lugworms) mixed-flat mud-draped current ripples (Facies 4.2) (River Esk cores 2A and 2B; central-basin cores 5A and 5B). **A)** Map of site for cores 2A and 2B (see Fig. 1B for location). **B)** Photograph of core site 2A. **C)** Photograph of core site 2B. **D)** Map of site for cores 5A and 5B (see Fig. 1B for location). **E)** Photograph of core site 5A. **F)** Photograph of core site 5B. **G)** Log for core 2A, with detrital-clay-coat coverage (red circles) and bioturbation index (BI) (grayed area) presented next to each schematic sedimentary log. **H)** Log for core 2B, including detrital-clay-coat coverage and bioturbation index. **I)** Log of core 5A, including detrital-clay-coat coverage and bioturbation index. **J)** Log of core 5B, including detrital-clay-coat coverage and bioturbation index. Note, that low-amplitude dunes and mixed-flat sediments overlay pyritized mud-flat sediments in the central basin. Refer to Table 2 for explanation of facies codes and Figure 2 for the classification of clay-coat coverage.



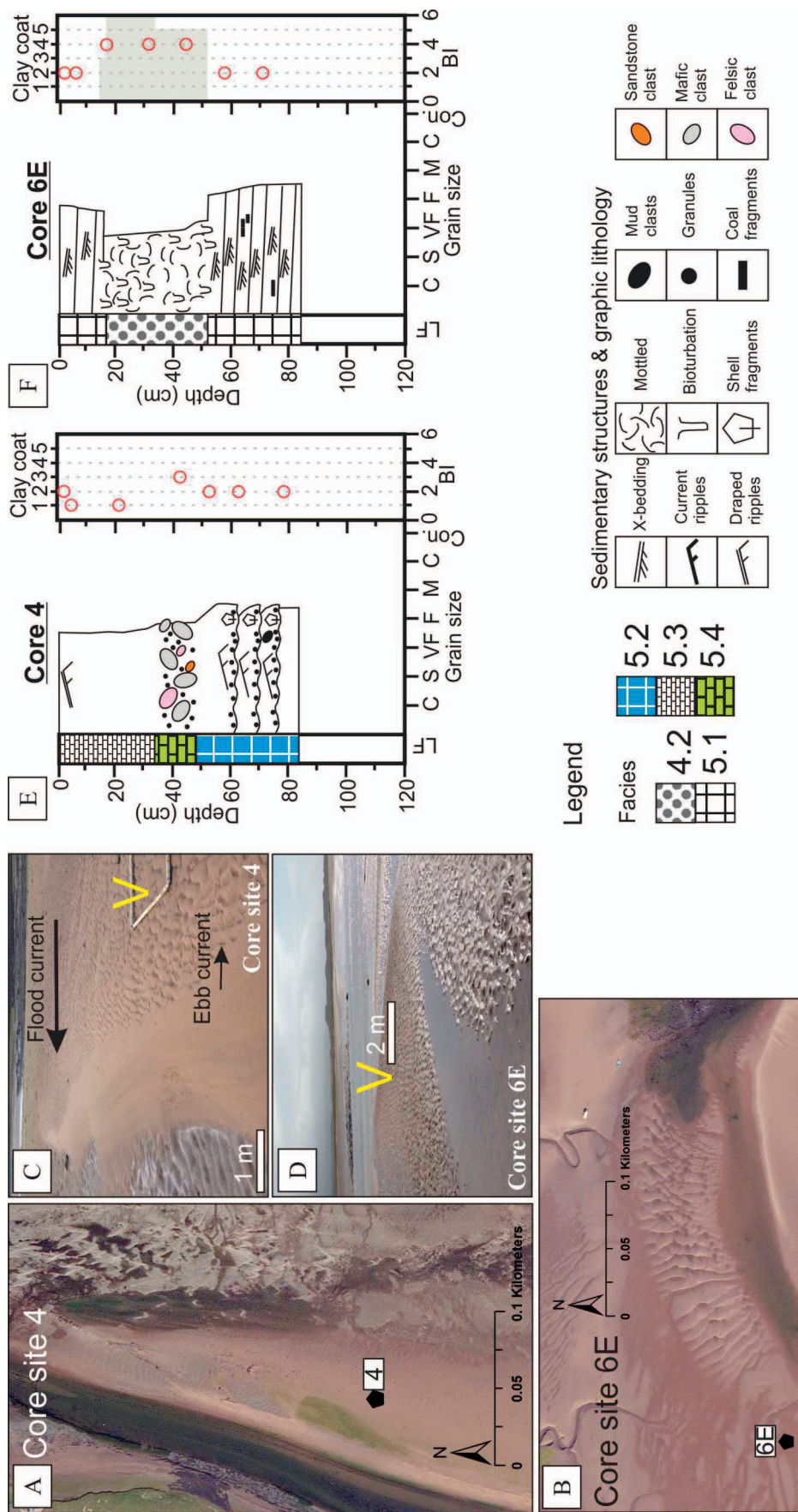


FIG. 9.—Core locations and schematic sedimentary logs of river Esk detached tidal-bar sediments (FA 5; core 4) and central-basin low-amplitude dunes (FA 5; core 6E) interbedded with bioturbated (primarily *Arenicola marina*; lugworms) mixed-flat sediments (Facies 4.2). **A)** Map of site for core 4 (see Fig. 1B for location). **B)** Map of site for core 6E (see Fig. 1B for location). **C)** Photograph of core site 4. **D)** Photograph of core site 6E. **E)** Log for core 4, with detrital-clay-coat coverage (red circles) and bioturbation index (BI) (grayed area) presented next to each schematic sedimentary log. **F)** Log for core 6E, including detrital-clay-coat coverage and bioturbation index. Refer to Table 2 for explanation of facies codes and Figure 2 for the classification of clay-coat coverage.



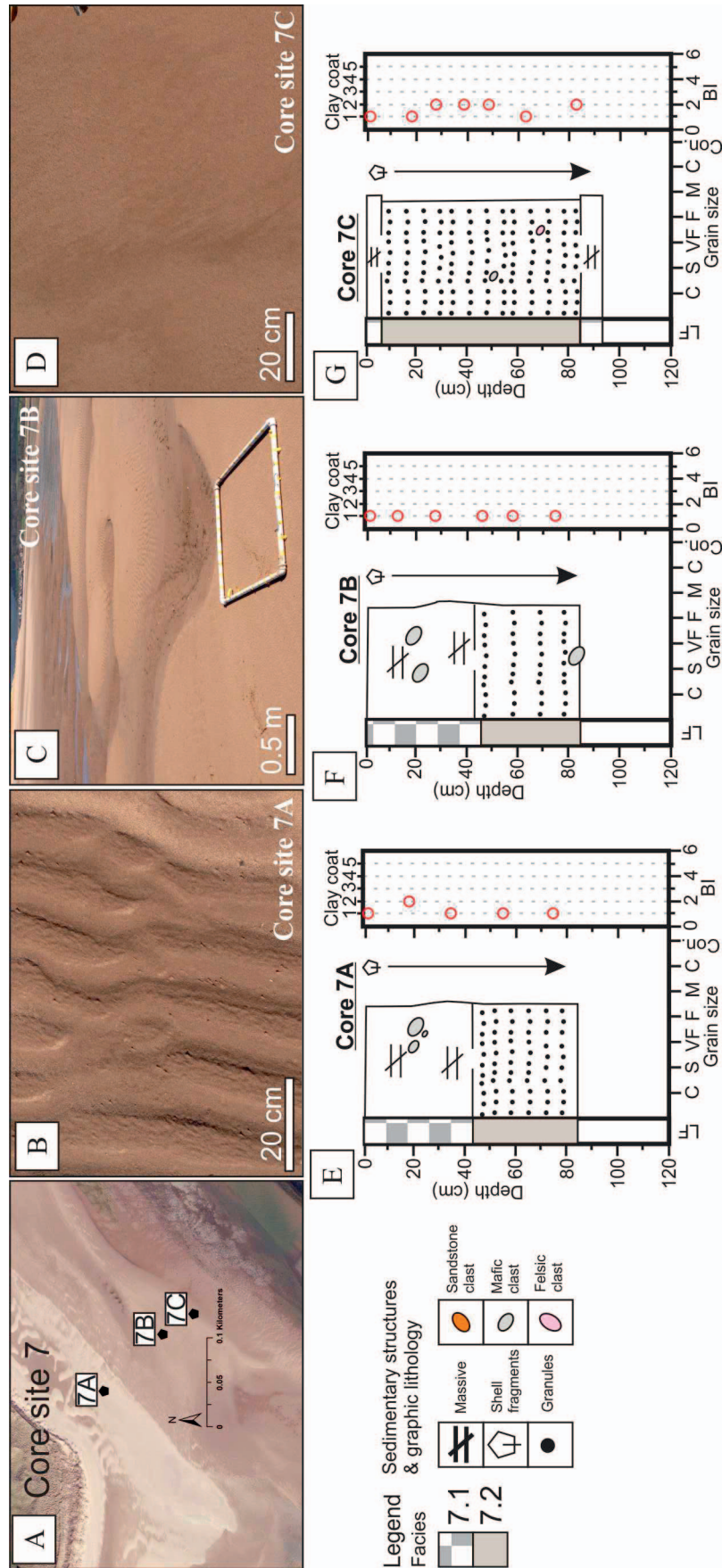
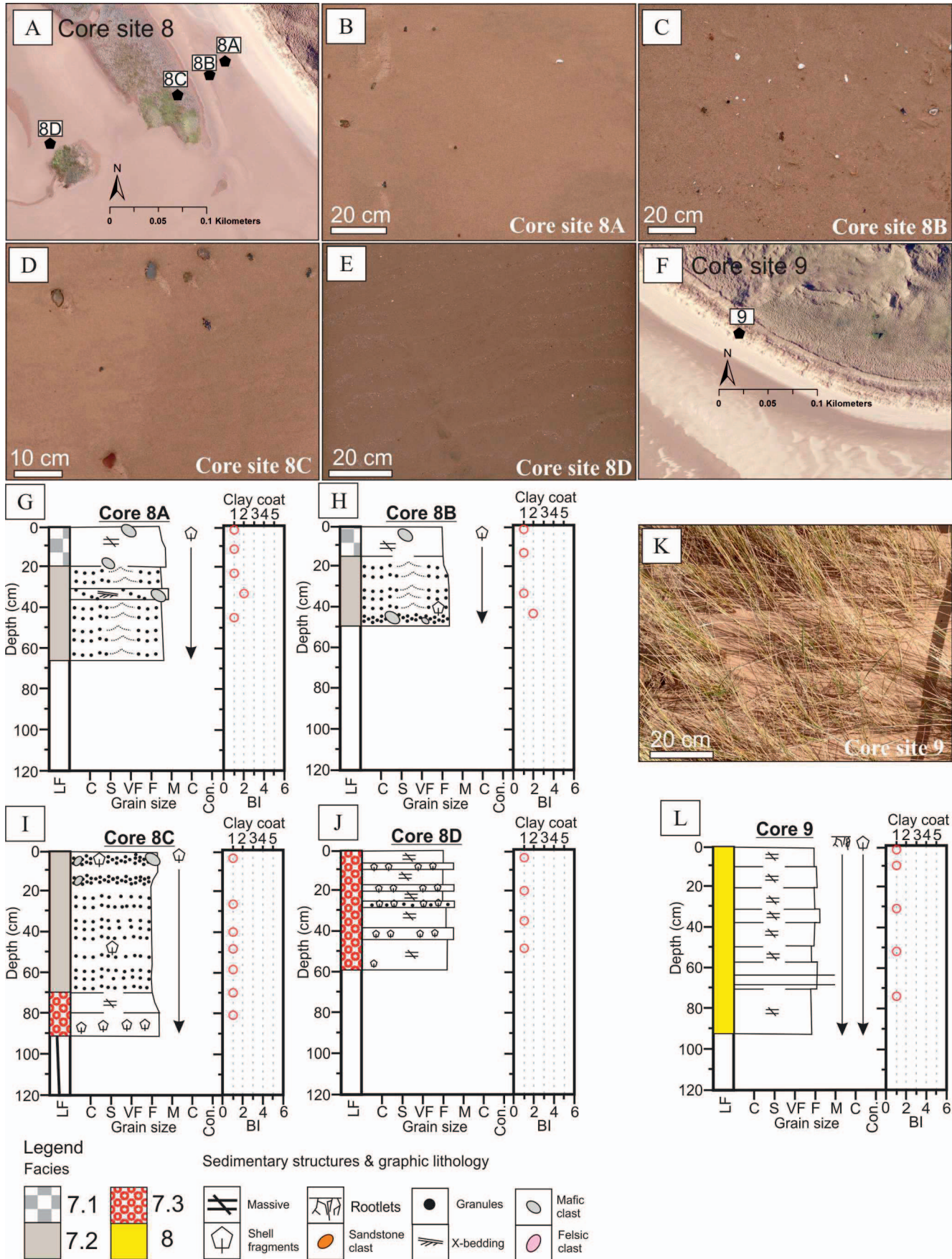


FIG. 10.—Core locations and schematic sedimentary logs of tidal-inlet sediments (FA 7: wave ripples, migratory 3D dunes, and upper-phase plane bed). **A)** Map of site for cores 7A to 7C (see Fig. 1B for location). **B)** Photograph of core site 7A. **C)** Photograph of core site 7B. **D)** Photograph of core site 7C. **E)** Log for core 7A with detrital-clay-coat coverage (red circles) and bioturbation index (BI) (grayed area) presented next to each schematic sedimentary log. **F)** Log for core 7B, including detrital-clay-coat coverage and bioturbation index. **G)** Log of core 7C, including detrital-clay-coat coverage and bioturbation index. Refer to Table 2 for explanation of facies codes and Figure 2 for the classification of clay-coat coverage.





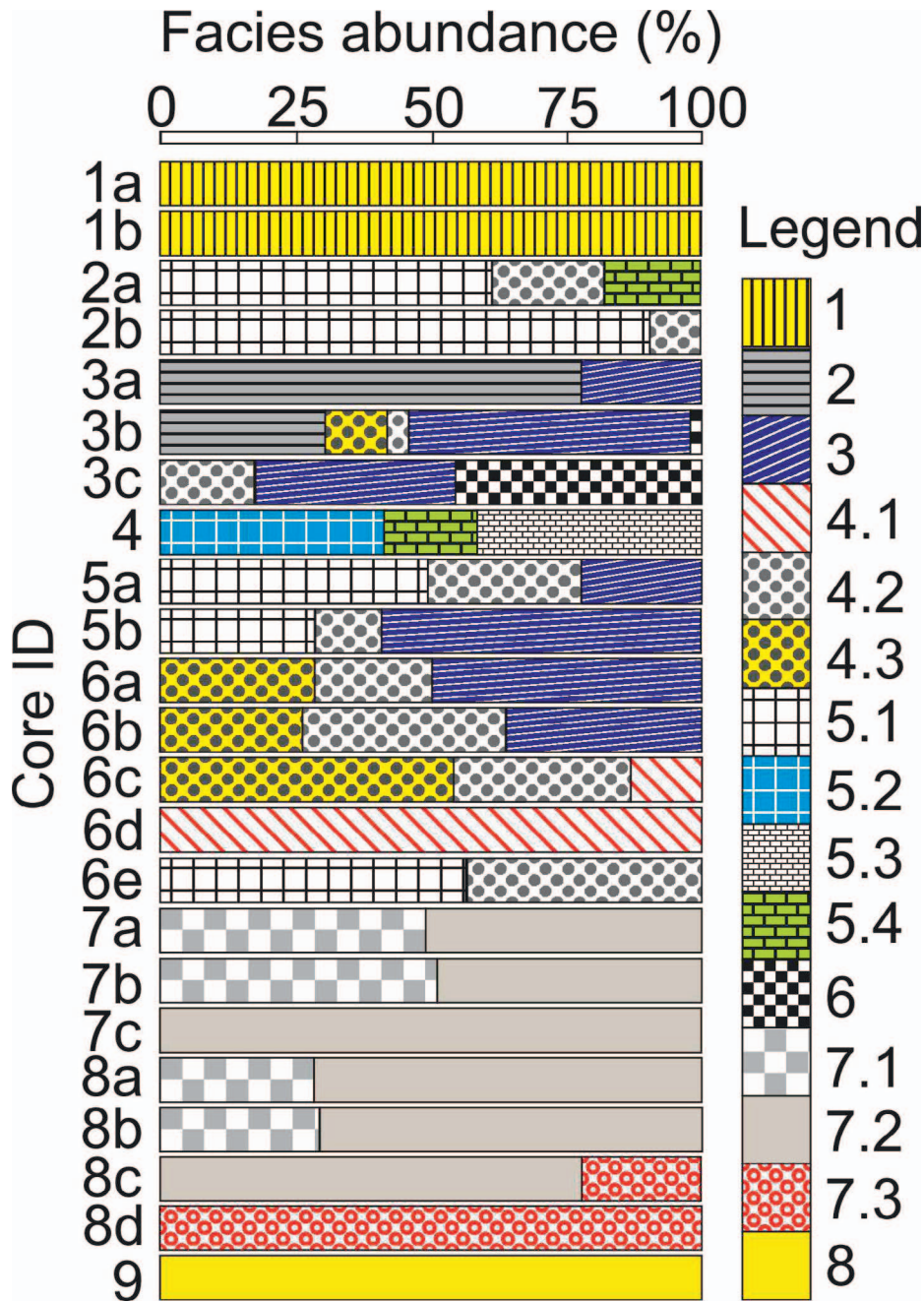


FIG. 12.—Facies type and abundance in each core. Refer to Table 2 for explanation of facies codes.

sample is shown in Figure 22. Chlorite abundance increases with an increase in grain size (Fig. 22). Illite and kaolinite abundances decrease with an increase in grain size (Fig. 22). Smectite is typically restricted to sediment fractions < 15 μm (Fig. 22).

**Mineralogy of Quaternary Drift Deposits**

X-ray diffraction analysis was performed on drift deposits exposed in the cliff sections in the inner Esk (Gosforth Glaciogenic Formation and Seascale Glaciogenic Formation), and from Ravenglass Till (part of the

Fig. 11.—Core locations and schematic sedimentary logs of foreshore (FA 7) and coastal-spit deposits (FA 8). Structureless upper-foreshore deposits (cores 8A and 8B) are separated by an approximately 1 m reduction in surface elevation (break in slope; see Fig. 1B) from swash-zone deposits with abundant granules and pebbles (core 8C) and wave-formed ripples draped by disarticulated shell-fragments (core 8D). Coastal spits consist of well-vegetated aeolian dunes (core 9; FA 8). **A)** Map of site for cores 8A and 8D (see Fig. 1B for location). **B)** Photograph of core site 8A. **C)** Photograph of core site 8B. **D)** Photograph of core site 8C. **E)** Photograph of core site 8D. **F)** Map of site for core 9 (see Fig. 1B for location). **G)** Log for core 8A, with detrital-clay-coat coverage (red circles) and bioturbation index (BI) (grayed area) presented next to each schematic sedimentary log. **H)** Log for core 8B, including detrital-clay-coat coverage and bioturbation index. **I)** Log of core 8C, including detrital-clay-coat coverage and bioturbation index. **J)** Log of core 8D, including detrital-clay-coat coverage and bioturbation index. **K)** Photograph of core site 9. **L)** Log of core 9, including detrital-clay-coat and bioturbation index. Refer to Table 2 for explanation of facies codes and Figure 2 for the classification of clay-coat coverage.

TABLE 2.—Diagnostic features (dominant texture, sedimentary structures, and ichnofabrics) of facies associations (FA) and lithofacies (LF; facies differentiated by diagnostic lithological features, such as texture and sedimentary structures) encountered in a wide range of depositional environments in the Ravenglass Estuary. See Figure 4 to view the surface expression and distribution for each FA.

Depositional Environment	Facies		Fig. N°	Surface Description	Diagnostic Near-Surface Characteristics						
	FA	Lf		Sedimentary Characteristics and Depositional Process	Dominant Texture and Sedimentary Structures	Dominant Ichnofabrics					
Fluvial floodplain	1	1	Fig. 5	Alluvium aggradation. Deposition of clay, silt, and sand during periods of overbank flooding (periods of high fluvial discharge and/or spring tide).	Vegetated, mottled silt to very fine-grained sand with sporadic (obscured) very fine-grained sand laminae.	Common rootlets and <i>Lumbricidae</i> (earthworm)					
Salt marsh	2	2	Fig. 6	Marine alluvium aggradation. Deposition of clay, silt, and sand during high tide.	Vegetated and bioturbated silt-grade sediment with cyclic (cm-scale) very fine-grained lamina.	Common rootlets and <i>Corophium volutator</i> (sand shrimp)					
Mud flat	3	3	Fig. 7	Deposition of clay and silt sediment through suspension settling during periods of low energy (e.g., slack water). Fine-grained laminae are deposit during periods of increased energy (e.g., spring tide, storm events), and are typically mottled by intense bioturbation.	Mottled, clay and silt size sediment with very fine sand filled burrows, and obscured very fine sand laminae.	Common <i>Corophium volutator</i> and pioneer salt marsh					
Mixed-flat and thin bedded sediments (TBS)	4	4.1	Fig. 7	Wavy bedding occurs when the mud layers typically fill the ripple troughs, and overlie the ripples crest. In contrast, wavy flaser bedding fail to form continuous layers, and occur when the mud flasers fill only the ripple troughs or only overlie the ripple crest. Deposition of wavy flaser-bedded or wavy-bedded heterolithics is dependent on tidal conditions and the relative amount of suspended load during deposition.	Very-fine grained wavy flaser bedding and wavy-bedded heterolithics, with variable bioturbation intensity.	Common <i>Corophium volutator</i> Rare <i>Arenicola marina</i>					
		4.2					Mixed flat	Fig. 7	Migration of tidal-current-generated ripples, draped with mud during periods of slack water (during low tide). Intense bioturbation ( <i>Corophium volutator</i> and <i>Arenicola marina</i> ) often leads to sediment homogenization (mottled texture).	Mud-rich, very fine-grained sand (~ 4% clay size fraction), with current-ripples draped in mud.	Common <i>Corophium volutator</i> and <i>Arenicola marina</i>
		4.3					TBS	Fig. 7	Minor incursions (erosional base) are likely to occur during periods of high energy within the inner estuary and central basin (e.g. storm events) and due to the progradation and retrogradation of mixed flats and mud flats.	Very-fine- to fine-grained thin-bedded deposits (typically, < 10 cm; ~ 3% clay fraction). The lower contacts of the incursions are typically bioturbated or erosive.	Common <i>Corophium volutator</i> and <i>Arenicola marina</i>
Low-amplitude dunes and tidal bars	5	5.1	Figs. 8 and 9	Migration of low-amplitude tidal dunes and current ripples, proximal to the ebb channel. Mud drapes are deposited during low tide.	Very fine- to medium-grained, cross-bedded and current-rippled sand with an erosional base (< 1% clay size fraction). Mud drapes are common.	Common <i>Arenicola marina</i>					
		5.2					Tidal bar (toesets and bottom sets)	Fig. 9	Migration of planar dunes, with the deposition of granules and shell fragments within the toesets and bottom-sets of planar dunes.	Fine- to medium-grained and sands with an erosional base, consisting of disarticulated shell fragments and granules.	Very rare <i>Arenicola marina</i>
		5.3					Tidal bar (dune crest)	Fig. 9	Deposition of fine-to medium-grained sand at the crests of migratory tidal dunes.	Very fine- to fine-grained sand with no discernible bedding structures	Very rare <i>Arenicola marina</i>
		5.4					Trough lag deposit	Fig. 9	Deposition of pebble-size material in the troughs of migratory tidal dunes.	Matrix-supported conglomerate (up to pebble size).	Absent



TABLE 2.—Continued.

Depositional Environment	Facies		Fig. N°	Surface Description	Diagnostic Near-Surface Characteristics	
	FA	Lf		Sedimentary Characteristics and Depositional Process	Dominant Texture and Sedimentary Structures	Dominant Ichnofabrics
Glacial armored surface	6	6	Fig. 6	Glacial outwash of sand and gravels at the end of the last glacial period.	Fe-stained clast-supported (pebble-size), conglomerate capped by a Fe-cemented layer (1 cm thick).	Absent
Tidal inlet and foreshore	7	7.1	Figs. 10 and 11	Sediment is deposited by wave- and tidal-currents and typically reworked by wind action. Surface sedimentary structures vary from upper-phase plane beds, 3D dunes, wave-ripples, and wind-blown surfaces.	Massive, fine to medium grained, lithic-rich sand. Pebbles are common. Note, some sedimentary structures may not be discernible due to the friable nature of sand-rich modern sedimentary cores.	Absent
		7.2	Figs. 10 and 11	Granule-rich sediment is primarily deposited during swash- and backwash. Shell-lag deposits are deposited in the trough of migratory 3D dunes.	Medium-grained sand, with granules deposited as lamina-sets, with frequent pebble and shell lag-deposits.	Absent
		7.3	Figs. 10 and 11	Wave action, which generated wave-formed ripples, draped in disarticulated shell-fragments (proximal to the mean low-water line).	Massive, carbonate-rich fine-grained sand.	Absent
Coastal spits	8	8	Fig. 11	Aeolian dune migration (partly-stabilised by dune-vegetation).	Very-fine- to fine-grained, massive, well-sorted sands (partly vegetated).	Absent

Seascale Glaciogenic Formation) exposed as knolls throughout the estuary. XRD analyses show the fine fraction ( $< 2 \mu\text{m}$ ) of the Ravenglass Till (part of the Seascale Glaciogenic Formation) is dominated by well-crystalline, Fe-Mg-enriched illite (illite index, 0.62; Esquevin index 0.28; illite crystallinity, 0.24), and has a low to moderate abundance of kaolinite (kaolinite index, 0.21) and chlorite (chlorite index, 0.17). XRD-analyses show the fine fraction ( $< 2 \mu\text{m}$ ) of the Fishgarth Wood Till Member (part of the Gosforth Glaciogenic Formation) is dominated by Al-enriched illite (illite index, 0.61; Esquevin index 0.43; illite crystallinity, 0.21), relatively enriched in kaolinite (kaolinite index, 0.31), and depleted in chlorite (chlorite index, 0.08).

## DISCUSSION

### *Estuarine Facies: Nature and Organization*

It is challenging to discriminate between tide-dominated and wave-dominated estuaries based on outcrop and subsurface data, due to the typical paucity of data (i.e., limited spatial resolution) (Davis and Dalrymple 2011). As a result, many reconstructions are likely to adhere too strictly to either wave- or tide-dominated models (Davis and Dalrymple 2011). Consequently, mixed-energy estuarine systems such as Ravenglass (this study) and Gironde (Allen and Posamentier 1994) are likely to be underreported in the stratigraphic record.

The dominant controls on the distribution of lithofacies in the Ravenglass Estuary (Figs. 4 to 11; Table 2) are in broad agreement with those reported in wave- and tide-dominated end-member estuarine models detailed by Dalrymple et al. (1992). The Drigg and Eskmeals coastal spits, diagnostic of wave-dominated estuaries (Dalrymple et al. 1992), provide shelter to the inner estuary and central basin from wave action. As a result the spits have led to a relatively quiescent central basin and the deposition of mud flats (Fig. 4; FA 3; Table 2), mixed flats and thin-bedded heterolithic deposits (Fig. 4; FA 4; Table 2). Strong tidal currents,

diagnostic of tide-dominated estuaries (Dalrymple et al. 1992), pass beyond the low-energy central basin into the upper estuary, leading to the deposition of low-amplitude dunes and tidal bars (Fig. 4; FA 5; Table 2). Tidal currents and wave action have led to the deposition of a suite lithofacies that are diagnostic of tidal inlet and outer-estuarine sub-environments (Fig. 4; FAs 7 and 8; Table 2). The lithofacies scheme (Table 2) presented in this study can be used, by analogy, in mixed-energy estuaries. However, as with previously published facies models, local variability might cause departure from the generalized descriptions.

### *Detrital Clay Coats: Origin and Distribution*

Clay-coat distribution patterns in near-surface sediment (this study;  $< 1 \text{ m}$ ) are consistent with those reported in surface sediment ( $< 2 \text{ cm}$ ) in the Ravenglass Estuary (Wooldridge et al. 2017a; Wooldridge et al. 2017b). The extent of detrital-clay-coat coverage in the near-surface sediment of the Ravenglass Estuary is directly related to the abundance of clay fraction in the sediment ( $r = 0.92$ ,  $p < 0.001$ ), which is at least partly controlled by estuarine hydrodynamics and thus predictable as a function of lithofacies (Table 4; Fig. 15). In agreement with Matlack et al. (1989), detrital-clay-coat coverage is absent or negligible in high-energy, coarser-grained, outer-estuarine depositional environments (e.g., foreshore, tidal inlet, and backshore) due to paucity of clay-size material (minimum suspended load). In contrast, detrital-clay-coat coverage is most extensive in low-energy, finer-grained, inner-estuary and central-basin depositional environments (e.g., mud flats and mixed flats), due to an abundance of clay-size material that was deposited during slack-water conditions (Fig. 15). Furthermore, diatoms are most abundant in the inner estuary and central basin (Wooldridge et al. 2017a); diatoms have been reported to physically attach clay-size material to sand grain surfaces by adhesive extracellular polymeric substances (biofilms) in the top few millimeters of the sediment surface (Wooldridge et al. 2017a; Wooldridge et al. 2018). Both

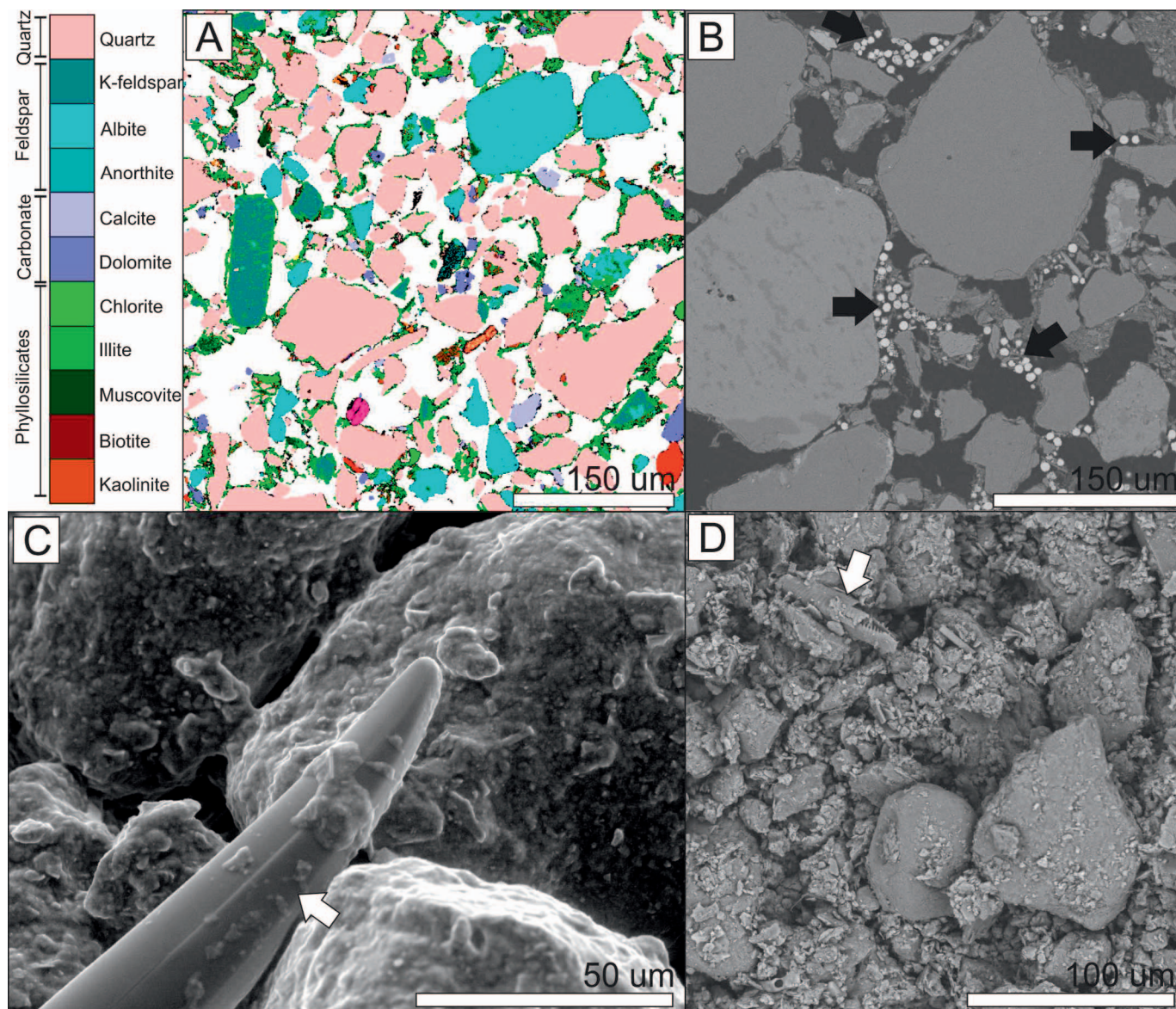


FIG. 13.—Clay-coat composition and pyrite and diatom presence in mixed-flat near-surface sediment. **A)** SEM-EDS (QEMSCAN®) analysis (micron-scale; 2  $\mu\text{m}$ ) revealing that clay minerals are the primary constituent in detrital grain coats and that most clay in the Ravenglass Estuary is present as clay coats. Note that SEM-EDS analysis revealed that chlorite is Fe-rich (chamosite). **B)** Backscattered electron (BSEM) analysis showing the presence and type of pyrite (highlighted by black arrows) typically hosted in detrital clay coats. **C)** Environmental scanning electron microscope (ESEM) image of hydrated near-surface sediment possibly being bound by extracellular polymeric substances secreted during diatom locomotion (possible mechanism for clay-coat development). **D)** Secondary electron (SE) image of dried sediment containing a diatom (highlighted by white arrows).

environmental scanning electron microscopy (ESEM) of hydrated sediment (Fig. 13C) and secondary electron microscopy (SE) of dried sediment (Fig. 13D) confirmed that diatoms are present in near-surface sediment in the Ravenglass Estuary. However, chemical evidence, such as Raman Spectroscopy (Wooldridge et al. 2017a), would be necessary to confirm the presence of biofilm. As a result, based on visual evidence of diatoms alone, this study cannot confirm whether or not clay coats have been mediated due to biofilms (extracellular polymeric substances exuded by diatoms) in near-surface sediment in the Ravenglass Estuary.

Clay coats have previously been reported to originate from the mechanical infiltration, or illuviation, of clay-laden waters in sediment (Matlack et al. 1989; Moraes and De Ros 1990; Pittman et al. 1992; Wilson 1992; Buurman et al. 1998). It has been proposed that infiltration

can occur on a centimeter to meter scale in marginal marine depositional environments (Santos et al. 2012), and therefore might lead to the overprinting of surface (< 2 cm) clay-coat distribution patterns in the near surface (< 1 m). However, the absence of a systematic increase or decrease in clay content with depth (Table 5) suggests that mechanical infiltration has not occurred. It is acknowledged that, in landscapes with a strong lateral groundwater movement, transport of clay can be oblique (Buurman et al. 1998), and might crosscut depositional facies (Morad et al. 2010). However, in the Ravenglass Estuary, depositional environments that are relatively clay-depleted at the surface (< 1%), and have the same lithofacies association down to 1 m, remain depleted in clay content throughout (Fig. 14). The absence of a systematic increase or decrease in clay content with depth (Table 5) suggests that mechanical infiltration of



TABLE 3.—Average clay fraction, clay mineral, Esquevin index, illite crystallinity and pyrite abundance in each lithofacies (standard deviation shown in brackets), as well as the weighted average (W.av) for clay fraction, clay mineral, Esquevin index, illite crystallinity, and pyrite abundance of the entire dataset. Refer to Table 2 for explanation of lithofacies codes.

Lithofacies Code	1	2	3	4.1	4.2	4.3	5.1	5.2
Number of Samples (n)	18	10	24	11	25	12	13	3
Clay fraction (%) (mean (sd))	13.7 (4.84)	22.6 (3.87)	12 (3.84)	4.6 (3.38)	4.3 (2.56)	2.7 (1.55)	0.6 (0.47)	0.6 (0.04)
Chlorite index (mean (sd))	0.19 (0.19)	0.18 (0.004)	0.18 (0.010)	0.17 (0.008)	0.18 (0.013)	0.18 (0.022)	0.20 (0.19)	0.18 (0.017)
Kaolinite index (mean (sd))	0.21 (0.020)	0.21 (0.012)	0.21 (0.012)	0.21 (0.011)	0.21 (0.010)	0.22 (0.014)	0.23 (0.009)	0.22 (0.015)
Illite index (mean (sd))	0.56 (0.017)	0.62 (0.014)	0.61 (0.016)	0.61 (0.011)	0.60 (0.020)	0.59 (0.037)	0.58 (0.023)	0.59 (0.032)
Smectite index (mean (sd))	0.04 (0.036)	0.00	0.01 (0.015)	0.00	0.00	0.01 (0.033)	0.00	0.00
Esquevin index (mean (sd))	0.29 (0.026)	0.30 (0.022)	0.29 (0.021)	0.31 (0.050)	0.30 (0.024)	0.31 (0.044)	0.33 (0.057)	0.32 (0.039)
Illite crystallinity (mean (sd))	0.23 (0.016)	0.24 (0.018)	0.25 (0.019)	0.25 (0.017)	0.25 (0.023)	0.25 (0.031)	0.27 (0.031)	0.27 (0.021)
Pyrite (%) (mean (sd))	0.00	0.00	0.55 (0.637)	0.28 (0.462)	0.76 (1.227)	0.17 (0.389)	0.71 (1.369)	0.00
Lithofacies Code	5.3	5.4	6	7.1	7.2	7.3	8	Weighted Average
Number of Samples (n)	3	1	1	11	21	6	5	
Clay fraction (%) (mean (sd))	0.3 (0.016)	0.5 (n/a)	0.5 (n/a)	0.1 (0.07)	0.1 (0.04)	0.1 (0.02)	0.1 (0.04)	5.9
Chlorite index (mean (sd))	0.19 (0.007)	0.21 (n/a)	0.21 (n/a)	0.24 (0.016)	0.24 (0.022)	0.21 (0.018)	0.24 (0.011)	0.20
Kaolinite index (mean (sd))	0.22 (0.017)	0.23 (n/a)	0.19 (n/a)	0.23 (0.020)	0.21 (0.016)	0.22 (0.013)	0.21 (0.019)	0.21
Illite index (mean (sd))	0.59 (0.022)	0.55 (n/a)	0.60 (n/a)	0.53 (0.028)	0.55 (0.028)	0.58 (0.021)	0.55 (0.025)	0.58
Smectite index (mean (sd))	0.00	0.23 (n/a)	0.00	0.00	0.00	0.00	0.00	0.01
Esquevin index (mean (sd))	0.29 (0.014)	0.31 (n/a)	0.23 (n/a)	0.31 (0.033)	0.31 (0.047)	0.33 (0.051)	0.29 (0.046)	0.30
Illite crystallinity (mean (sd))	0.31 (0.006)	0.29 (n/a)	0.26 (n/a)	0.25 (0.040)	0.25 (0.026)	0.26 (0.010)	0.29 (0.021)	0.25
Pyrite (%) (mean (sd))	0.00	0.00	0.00	0.00	0.00	0.00	0.00	0.29

clay has not occurred in significant quantities to overprint surface detrital-clay-coat distribution patterns reported by Wooldridge et al. (2017a). Furthermore, in an experimental study by Matlack et al. (1989), which showed clay coats can develop through mechanical infiltration, relatively high percolation speeds were achieved for the suspended clays (through the sand-pack columns due to free gravity-induced flow) which is unrepresentative of estuarine depositional environments (Buurman et al. 1998). For example, under natural conditions, reduced flow velocities will lead to

minerals flocculating, subsequently deposited as mud drapes, which are seen to clog the upper pore throats of the sediment and inhibit the infiltration of clay-laden water further into the sediment subsurface (e.g., Fig. 8; cores 2A–B and 5A–B). It is noteworthy that clay flocculation is especially common in marginal-marine systems, due to increased salinity at the fluvial–marine interface (Chamley 1989). Furthermore, clay-rich layers create impermeable barriers in tidal flats, which form a baffle to

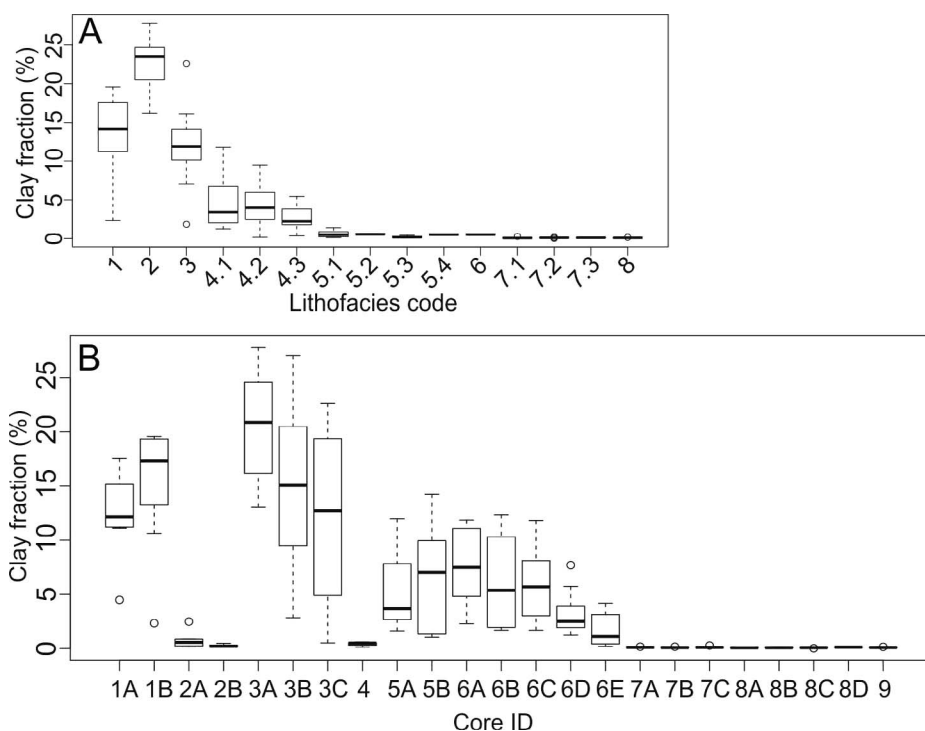


FIG. 14.—Clay-fraction abundance (%) as a function of A) lithofacies and B) core ID (core position). Refer to Table 2 for explanation of lithofacies codes.

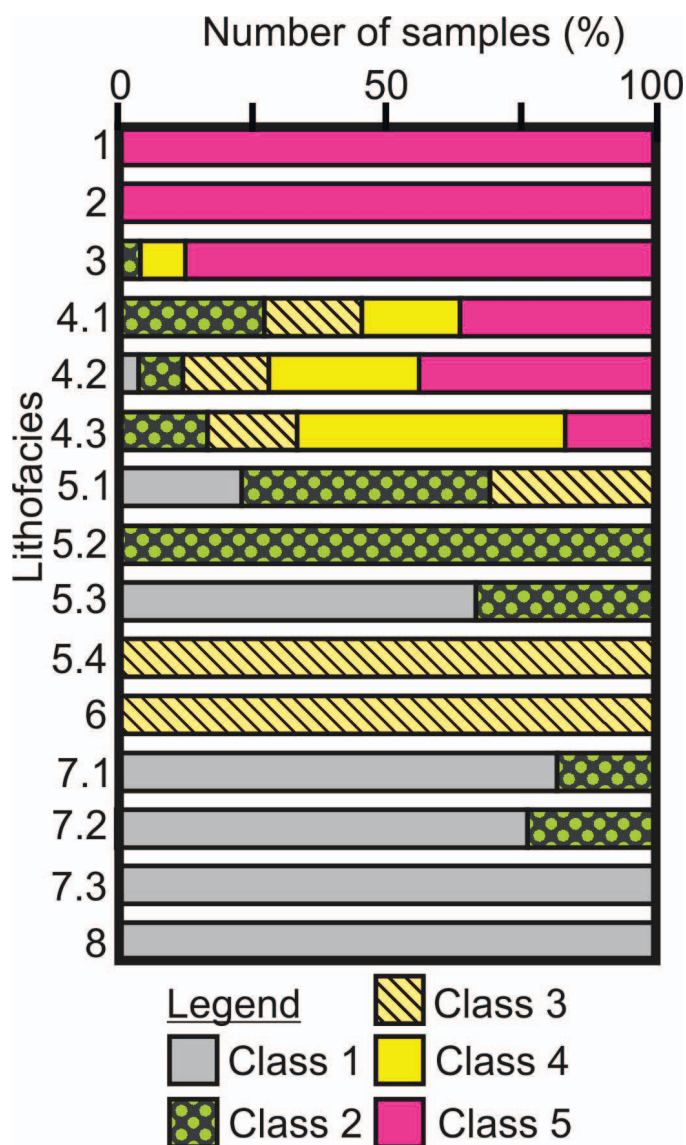


FIG. 15.—Clay-coat class (1–5) abundance in each lithofacies. Clay-coat classes are defined as follows, after Wooldridge et al. (2017b): (Class 1) Complete absence of clay coats. (Class 2) Less than half of the grains have a small (~ 1–5 %) surface area of attached clay coats. (Class 3) Every grain exhibits at least ~ 5–15 % clay-coat coverage (Class 4) Extensive (~ 15–30 %) clay-coat coverage on the majority of grains. (Class 5) Greater than 30% surface area covered by clay coats on every grain. Refer to Table 2 for explanation of lithofacies codes.

mechanical infiltration, often resulting in the formation of fluidized mud layers at the surface.

Experimental studies have shown that detrital clay coats can develop through the direct ingestion and excretion of sediment by *Arenicola marina* (lugworms) (Needham et al. 2005; Worden et al. 2006). However, *Arenicola marina* are restricted to a limited environmental grain-size niche in the Ravenglass Estuary, typically 88 to 177  $\mu\text{m}$  (Wooldridge et al. 2017b), and are not present in mud flats, where clay coats are most abundant (Fig. 15). Therefore, in agreement with distribution patterns presented by Wooldridge et al. (2017b), clay-coat distribution patterns in near-surface sediment also do not appear to be determined exclusively by the bioturbation of *Arenicola marina*. However, in contrast to Wooldridge et al. (2017b), in this study we have measured the bioturbation signal of all

fauna, and not just the castings developed by *Arenicola marina*; there is a strong correlation between bioturbation index (signal from all microfauna and macrofauna) and clay-coat coverage ( $r = 0.84$ ,  $p < 0.001$ ). As reported by Wooldridge et al. (2017b), it might be possible that other estuarine macro- or micro-organisms provide a mechanism of clay coat formation. *Corophium volutator* (which create densely spaced U-shaped burrows up to 5 cm deep) are confined to mud flats and mixed flats in the Ravenglass Estuary (Kelly et al. 1991), and thus correspond to high degrees of detrital-clay-coat coverage. Previous studies have also reported that *Corophium volutator* can occur in abundance up to  $140,000 \text{ m}^{-3}$  in estuarine mudflats and salt marsh (Gerdol and Hughes 1994). However, despite the striking similarity between bioturbation intensity (primarily through *Corophium volutator* activity in mud flats and mixed flats) and detrital-clay-coat coverage, *Corophium volutator* are unlikely to have formed clay coats. First, *Corophium volutator* are reported to increase the water content of sediment and thus decrease shear strength and promote erosion and winnowing of sediment (Gerdol and Hughes 1994), which are all likely to remove clay coats. Second, *Corophium volutator* are reported to consume diatoms in marginal-marine sediments (Underwood and Paterson 1993; Gerdol and Hughes 1994), which are known to adhere clay-size material to sand grain surfaces via biofilms (Jones 2017; Wooldridge et al. 2017a). As a result, despite there being a strong correlation between macrofaunal bioturbation intensity (primarily by *Corophium volutator* in clay-rich depositional environments with the most extensive detrital clay coat coverage) and detrital-clay-coat coverage, *Corophium volutator* might in fact inhibit detrital clay coat development through the reduction of diatom populations. Instead, the strong correlation between bioturbation index and the extent of detrital-clay-coat coverage is more likely driven by: (i) the absence of both clay coats and bioturbation in outer-estuarine sediment, (ii) a high abundance of burrowing *Corophium volutator* and clay-grade material in mud flats.

In summary, detrital-clay-coat distribution patterns in estuarine near-surface (< 1 m) sediment are likely controlled by processes active during deposition and in the top few centimeters of the primary deposition environment; the physical sorting of sediment by grain size via estuarine hydrodynamics, and the adhesion of clay to sand grain surfaces by biofilms secreted by diatoms (Wooldridge et al. 2017a). Thus, detrital-clay-coat distribution patterns in surface sediment (< 2 cm) in the Ravenglass Estuary have not been overprinted by postdepositional processes.

#### Clay Mineralogy: Origin and Controls on Distribution

To better predict the distributions of authigenic and detrital clay minerals in sandstones reservoirs, it is necessary to understand the fundamental controls on the type and occurrence of detrital clay minerals in the primary depositional environment. Chlorite, illite, kaolinite, and smectite are not homogeneously distributed in the Ravenglass Estuary (Figs. 16–21). In this section, the principal controls on the clay-mineral assemblage and clay-mineral distribution patterns in the Ravenglass Estuary are discussed.

#### Origin of Clay Minerals in the Ravenglass Estuary

Matching global oceanic clay-mineral trends (Rateev et al. 2008), the proportions of illite, chlorite, and kaolinite in the Ravenglass Estuary are approximately 3:1:1 with a trace quantity of smectite (average smectite index of 0.009; maximum smectite index of 0.09) (Table 3). Illite, the dominant clay mineral in the Ravenglass Estuary, has an average Esquevin index of 0.30 and illite crystallinity of 0.25, representing relatively well-crystalline and Fe-Mg-rich illite (Kübler 1964; Esquevin 1969).

Potential sources of clay minerals in the Ravenglass Estuary include: (i) fluvial drainage of Paleozoic and Triassic bedrock and Quaternary drift, (ii) the landward displacement of littoral-zone sediment, (iii) internal erosion



TABLE 4.—Post-hoc Dunn test results (following a Kruskal-Wallis H test) reveal between which lithofacies there is a statistical difference in detrital-clay-coat coverage. Paired lithofacies which have a statistically significant difference in detrital-clay-coat coverage have significant values (z values) highlighted in bold. In contrast, pale numbers represent insignificant differences in clay-coat coverage between compared lithofacies. Levels of statistical significant are coded as follows; marginally significant (+) when  $p < 0.1$ , significant (\*) when  $p < 0.05$ , very significant (\*\*) when  $p < 0.01$ , extremely significant (\*\*\*) when  $p < 0.001$ . Gray values represent no significant difference when  $p > 0.1$ . Refer to Table 2 for explanation of lithofacies codes.

Detrital-Clay-Coat Coverage												
	1	2	3	4.1	4.2	4.3	5.1	5.2	5.3	7.1	7.2	7.3
2	0	x										
3	0.47	0.39	x									
4.1	<b>2.23+</b>	1.96	1.95	x								
4.2	<b>2.23+</b>	1.84	1.9	-0.46	x							
4.3	<b>2.54*</b>	<b>2.21+</b>	<b>2.27+</b>	0.22	0.74	x						
5.1	<b>4.74***</b>	<b>4.1***</b>	<b>4.58***</b>	<b>2.12+</b>	<b>3.03**</b>	1.94	x					
5.2	<b>2.7*</b>	<b>2.56*</b>	<b>2.51*</b>	1.28	1.63	1.14	-0.06	x				
5.3	<b>3.49**</b>	<b>3.31**</b>	<b>3.32**</b>	2.03	<b>2.44*</b>	1.91	0.71	0.6	x			
7.1	<b>5.99***</b>	<b>5.24***</b>	<b>5.89***</b>	<b>3.37***</b>	<b>4.43***</b>	<b>3.22**</b>	1.38	0.93	0.17	x		
7.2	<b>7***</b>	<b>5.85***</b>	<b>7.04***</b>	<b>3.75***</b>	<b>5.27***</b>	<b>3.6**</b>	1.49	0.91	0.11	-0.11	x	
7.3	<b>5.14***</b>	<b>4.7***</b>	<b>4.99***</b>	<b>3.09***</b>	<b>3.82**</b>	<b>2.95*</b>	1.42	1.04	0.35	0.27	0.38	x
8	<b>4.8***</b>	<b>4.43***</b>	<b>4.63***</b>	<b>2.91***</b>	<b>3.54**</b>	<b>2.77*</b>	1.33	1.01	0.34	0.25	0.35	0

of Ravenglass Till that is exposed as knolls throughout the estuary and in proximal cliff sections.

The principal source of chlorite is probably the Eskdale Granite and Borrowdale Volcanic Group, because intense chloritization of mafic silicates has been reported in the Eskdale Granite (Moseley 1978; Young et al. 1986; Quirke et al. 2015) and widespread chloritization of pyroxene has been reported in the Borrowdale Volcanic Group (Quirke et al. 2015).

The provenance of illite in the Ravenglass Estuary has been established using Esquevin Indices. Illite in this estuary is relatively well-crystalline and Fe-Mg-rich (Figs. 18A, B, 20A, B); this is typical of cold-climate conditions that favor mechanical weathering allowing the primary white mica to retain its Fe-Mg-rich composition and original high degree of crystallinity (Chamley 1989). The chemical composition of illite in estuarine sediment (average Esquevin index of 0.30) compare closely with values calculated for the Ravenglass Till (average Esquevin index of 0.28).

TABLE 5.—Correlation (Spearman’s and Pearson’s correlation coefficients) between clay-mineral indices, pyrite abundance, clay-content and clay-coat coverage as a function of depth (per core). Bold numbers represent significant correlation coefficients, whereas pale numbers represent insignificant differences, in clay-mineral attributes (and pyrite) with depth. “x” represents values that were either absent or uniform with depth. Levels of statistical significant are coded as follows; marginally significant (+) when  $p < 0.1$ , significant (\*) when  $p < 0.05$ , very-significant (\*\*) when  $p < 0.01$ , extremely significant (\*\*\*) when  $p < 0.001$ . Gray values represent no significant difference when  $p > 0.1$ .

Core	Pearson’s					Spearman’s
	Chlorite Index	Illite Index	Kaolinite Index	Pyrite	Clay Fraction	Clay Coat
1a	<b>-0.72*</b>	0.20	<b>-0.86**</b>	x	0.14	x
1b	<b>-0.95***</b>	-0.17	<b>-0.99***</b>	x	<b>0.83**</b>	x
2a	0.63	-0.70	0.75	0.66	-0.55	-0.05
2b	0.62	-0.49	0.25	0.69	<b>-0.91**</b>	<b>-0.93**</b>
3a	-0.12	-0.11	0.17	x	-0.17	x
3b	-0.11	<b>-0.64+</b>	-0.76	x	<b>-0.63+</b>	-0.52
3c	0.69	0.21	-0.76	x	-0.88	-0.77
4	0.10	-0.23	0.38	x	<b>0.71+</b>	0.36
5a	-0.59	<b>0.73*</b>	<b>-0.84**</b>	-0.92	<b>0.76*</b>	0.32
5b	-0.36	0.57	<b>-0.74*</b>	-0.38	<b>0.92***</b>	<b>0.86**</b>
6a	0.31	0.14	0.10	<b>0.81**</b>	-0.52	-0.34
6b	<b>0.88**</b>	0.13	-0.54	<b>0.91**</b>	<b>0.87**</b>	0.11
6c	0.22	0.21	<b>-0.68*</b>	x	<b>-0.76*</b>	<b>-0.87**</b>
6d	-0.27	<b>-0.57+</b>	<b>0.79**</b>	<b>0.74**</b>	-0.45	<b>-0.68*</b>
6e	0.42	-0.44	0.43	x	-0.04	0
7a	0.55	-0.59	0.58	x	0.80	-0.35
7b	0.08	0.38	-0.65	x	0.44	x
7c	<b>0.74+</b>	<b>-0.84*</b>	<b>-0.84*</b>	x	<b>0.85*</b>	0.43
8a	-0.28	0.44	-0.46	x	<b>0.89*</b>	0.35
8b	<b>0.94+</b>	0.06	-0.67	x	0.83	0.77
8c	0.07	-0.13	0.11	x	0.47	x
8d	0.29	-0.26	0.13	x	0.50	x
9	-0.33	0.23	-0.11	x	-0.66	x

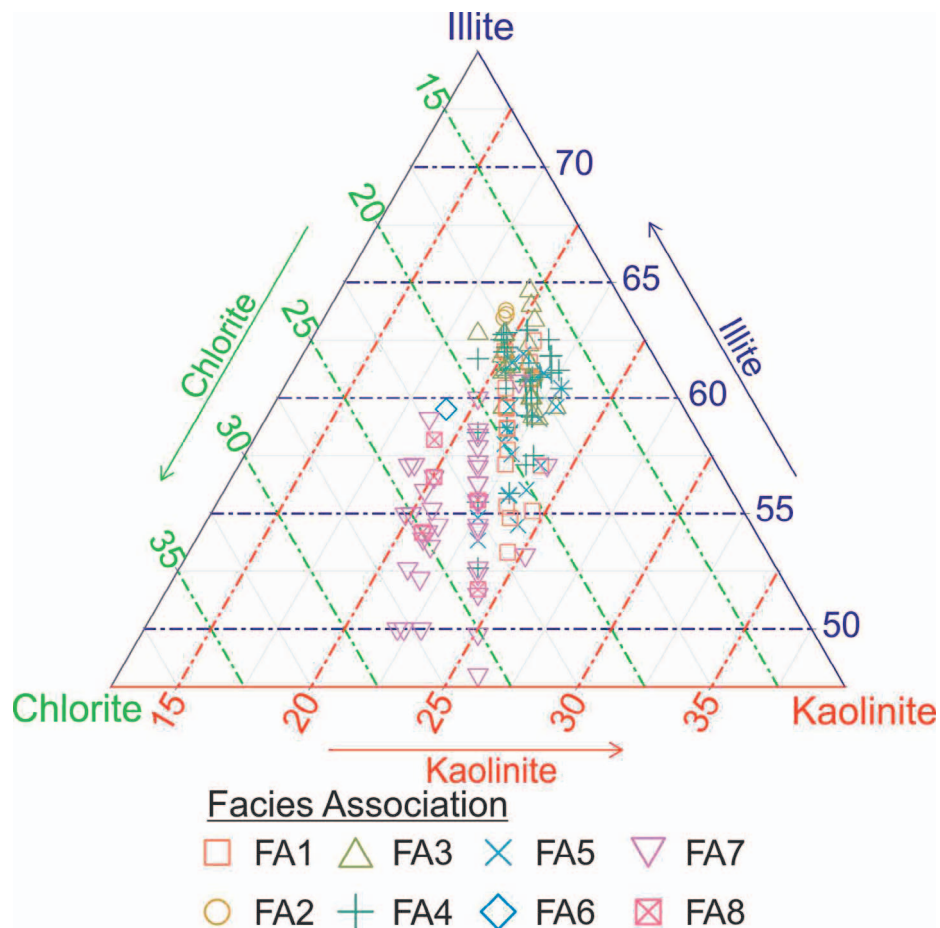


FIG. 16.—Relative clay-mineral abundance (illite, chlorite, kaolinite) as a function of facies association (FA). FAs are labelled accordingly: FA1, floodplain; FA2, salt marsh; FA3, mud flat; FA4, mixed-flat and thin-bedded deposits; FA5, low-amplitude tidal dunes and tidal bars; FA6, glacial outwash; FA7, tidal inlet and foreshore; and FA8, coastal spit.

The evidence therefore suggests that the dominant source of illite in the Ravenglass Estuary is the Ravenglass Till, which is relatively well exposed throughout the estuary and in the drainage basin. Al-rich illite, which is found primarily in outer-estuarine sediment, is characteristic of chemically weathered rocks that have lost Fe and Mg (Chamley 1989). Al-rich illite might reflect the widespread alteration of feldspars to fine-grained aluminous clay minerals (i.e., illite and kaolinite), which has been reported in the Eskdale Granite (Simpson 1934; Young et al. 1986; Quirke et al. 2015) and the Borrowdale Volcanic Group (Quirke et al. 2015).

Kaolinite might have been derived from the chemical weathering of any silicate minerals in the hinterland or in the Ravenglass Estuary basin. However, it is noteworthy that the glaciofluvial and glaciolacustrine sediments of the Fishgarth Wood Till Member (Fig. 1D) are relatively enriched in kaolinite (kaolinite index, 0.31) and so might provide a dominant source of kaolinite in the estuarine sediment.

Smectite, which is of minor abundance in the Ravenglass Estuary (average smectite index of 0.009), is typical of the initial stages of chemical weathering (Salem et al. 2000). In addition, weathering will only result in smectite, rather than other clay minerals, if the excess metal cations and silica cannot be flushed from the aqueous geochemical system, for example, in low-lying topography with poor drainage and stagnant groundwater conditions (McKinley et al. 2003). In contrast, in flowing and active groundwater systems, loss of metal cations is easily achieved, resulting in the possibility of more advanced chemical weathering and reduced preservation potential of smectite minerals (McKinley et al. 2003). As a result, smectite is most abundant, but still of relatively minor significance (smectite index of 0.09), in floodplain sediments of the River Esk (Fig. 19), analogous to the formation of dioctahedral smectite

downslope of weathered granitic rocks of the French Armorican Massif (Aoudjit et al. 1995).

#### *Clay-Mineral Distribution: Estuarine Hydrodynamics*

Similar to estuaries worldwide (Dalrymple et al. 1992), estuarine hydrodynamics has a profound influence on the nature and organization of lithofacies in the Ravenglass Estuary. Clay minerals can be physically sorted, due to grain-size variation, in marine environments during transport, as reported in Atlantic Ocean sediment influenced by the Amazon River (Gibbs 1977). This study has shown that hydrodynamic processes appear to have exerted a strong control on the distribution of lithofacies and specific clay minerals in the Ravenglass Estuary (Figs. 17, 18; Table 6).

Chlorite abundance typically increases with an increase in sediment grain size (Fig. 22). As a result, chlorite is relatively most abundant in high-energy and coarser-grained depositional environments, i.e., outer-estuarine sediment (lithofacies 7.1, 7.2, and 8; Fig. 17A) and in some inner-estuarine and central-basin low-amplitude-dune sediments (lithofacies 5.1; Fig. 17A). It is noteworthy that chlorite abundance appears to decrease toward the mean-low-water line in foreshore sediment (in lithofacies 7.3; Fig. 17A). Floodplain sediments are some of the finest-grained sediments in the estuary basin and could be expected to be chlorite-depleted (Fig. 22). However, floodplain sediments are relatively enriched in chlorite (chlorite index up to 0.25; Fig. 17A); this might reflect the fluvial deposition of chlorite-enriched River Esk sediment which drains the chloritized Eskdale Granite.



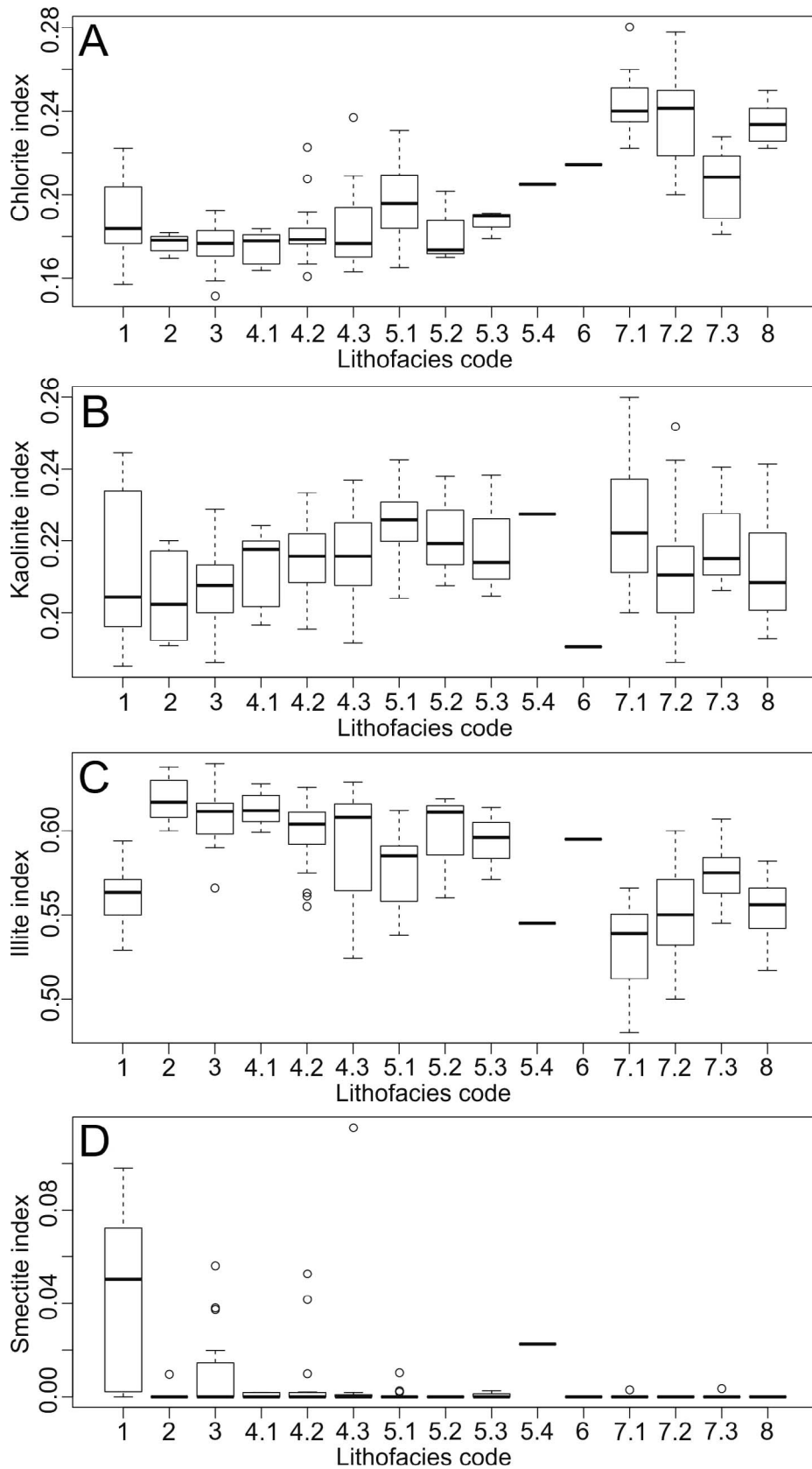


FIG. 17.—Relative clay-mineral abundance as a function of lithofacies. **A)** Chlorite index, **B)** kaolinite index, **C)** illite index, and **D)** smectite index. Refer to Table 2 for explanation of lithofacies codes.

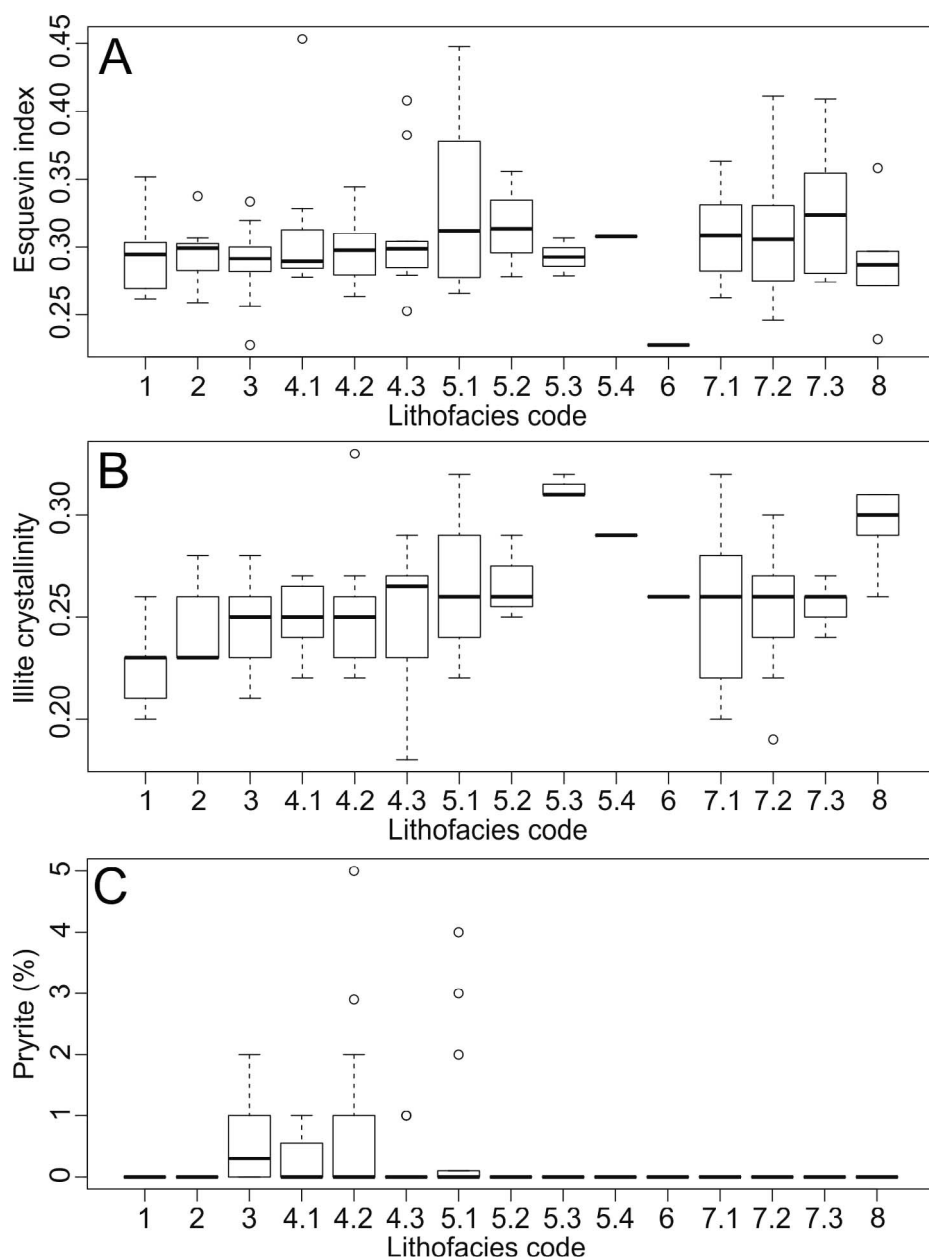


FIG. 18.—Variation in illite chemistry, illite crystallinity, and pyrite abundance as a function of lithofacies. **A**) Esquevin index, **B**) illite crystallinity, and **C**) pyrite abundance. Refer to Table 2 for explanation of lithofacies codes.

In the Ravenglass Estuary, illite is most abundant in finer-grained sediment (Fig. 22), and therefore illite enrichment occurs in sediment that is deposited under relatively quiescent conditions at the margin of the inner estuary and the central basin (Fig. 17C). However, estuarine hydrodynamics not only appear to control illite abundance, but also segregate illite by chemical composition and crystallinity (Fig. 18A, B). Well-crystalline Fe-Mg-rich illite is most abundant in finer-grained sediment, at the margin of the inner estuary and the central basin. In contrast, poorly crystalline Al-rich illite is most abundant in relatively high-energy inner-estuarine and central-basin lithofacies, such as low-amplitude dunes, as well as in outer-estuarine sediment. Fe-Mg-rich illite might be finer-grained than Al-rich illite due to Fe-Mg-rich illite being derived from sediment which has undergone extensive subglacial comminution (Ravenglass Till). Therefore, it is here speculated that the transport history of illite (intensity of abrasion and thus grain size) and estuarine hydrodynamics might also govern the distribution of illite types in the Ravenglass Estuary.

Kaolinite has been reported to flocculate at lower salinity than other clay minerals, and therefore is suggested to increase in abundance relative to other clay minerals at the fluvial-marine interface (Whitehouse et al. 1960). Kaolinite is reported to be deposited upstream relative to illite due to a faster aggregation rate (Edzwald and O'Mella 1975). However, in the Ravenglass Estuary there is no evidence for enrichment of kaolinite at the head of the estuary (Figs. 17B, 19B). Instead, kaolinite abundance is relatively homogeneous throughout the Ravenglass Estuary. Differential settling therefore does not appear to have exerted a strong control on kaolinite distribution in the Ravenglass Estuary. The effect of differential settling might be damped by strong tidal currents, wind, and a short-estuarine length promoting intense estuarine mixing resulting in a less well-defined fluvial-marine interface.

Smectite is present in the hinterland and in cores in the River Esk floodplain; however smectite is present in negligible abundance in Ravenglass estuarine sediments. There are two possible scenarios which might explain the paucity of smectite in estuarine sediments. First, smectite



TABLE 6.—Post-hoc Tukey HSD test results (following an ANOVA test) revealing between which lithofacies there is a statistical difference in chlorite, illite, kaolinite, and smectite abundance. Significant values (z values) are highlighted in bold. Bold numbers represent significant differences; pale numbers represent insignificant differences, in clay-mineral indices between compared depositional environments. Levels of statistical significant are coded as follows; marginally significant (+) when  $p < 0.1$ , significant (\*) when  $p < 0.05$ , very significant (\*\*) when  $p < 0.01$ , extremely significant (\*\*\*) when  $p < 0.001$ . Gray values represent no significant difference when  $p > 0.1$ . Refer to Table 2 for explanation of lithofacies codes.

Chlorite Index												
	1	2	3	4.1	4.2	4.3	5.1	5.2	5.3	7.1	7.2	7.3
2	-0.01	x										
3	-0.01	0	x									
4.1	-0.01	0	0	x								
4.2	-0.01	0	0.01	0.01	x							
4.3	0	0.01	0.01	0.01	0	x						
5.1	0.01	0.02	0.02	<b>0.02*</b>	0.02	0.01	x					
5.2	0	0.01	0.01	0.01	0	0	-0.02	x				
5.3	0	0.01	0.01	0.01	0.01	0	-0.01	0	x			
7.1	<b>0.06***</b>	<b>0.07***</b>	<b>0.07***</b>	<b>0.07***</b>	<b>0.06***</b>	<b>0.06***</b>	<b>0.05***</b>	<b>0.06***</b>	<b>0.06***</b>	x		
7.2	<b>0.05***</b>	<b>0.06***</b>	<b>0.06***</b>	<b>0.06***</b>	<b>0.06***</b>	<b>0.05***</b>	<b>0.04***</b>	<b>0.06***</b>	<b>0.05***</b>	-0.01	x	
7.3	0.02	<b>0.03*</b>	<b>0.03**</b>	<b>0.03*</b>	<b>0.02+</b>	0.02	0.01	0.02	0.02	<b>-0.04***</b>	<b>-0.03**</b>	x
8	<b>0.05***</b>	<b>0.06***</b>	<b>0.06***</b>	<b>0.06***</b>	<b>0.05***</b>	<b>0.05**</b>	<b>0.04**</b>	<b>0.05**</b>	<b>0.05**</b>	-0.01	0	0.03
Illite Index												
	1	2	3	4.1	4.2	4.3	5.1	5.2	5.3	7.1	7.2	7.3
2	<b>0.06***</b>	x										
3	<b>0.05***</b>	-0.01	x									
4.1	<b>0.05***</b>	0	0.01	x								
4.2	<b>0.04***</b>	-0.02	-0.01	-0.01	x							
4.3	<b>0.03***</b>	-0.03	-0.02	-0.02	-0.01	x						
5.1	0.02	<b>-0.04**</b>	<b>-0.03**</b>	<b>-0.04**</b>	-0.02	-0.01	x					
5.2	0.04	-0.02	-0.01	-0.02	0	0.01	0.02	x				
5.3	0.03	-0.02	-0.01	-0.02	-0.01	0	0.02	0	x			
7.1	<b>-0.03*</b>	<b>-0.09***</b>	<b>-0.08***</b>	<b>-0.08***</b>	<b>-0.07***</b>	<b>-0.06***</b>	<b>-0.05***</b>	<b>-0.07***</b>	<b>-0.06***</b>	x		
7.2	-0.01	<b>-0.07***</b>	<b>-0.06***</b>	<b>-0.06***</b>	<b>-0.05***</b>	<b>-0.04***</b>	<b>-0.03***</b>	<b>-0.05+</b>	-0.04	0.02	x	
7.3	0.01	<b>-0.04*</b>	<b>-0.03+</b>	<b>-0.04+</b>	-0.02	-0.02	0	-0.02	-0.02	<b>0.04*</b>	0.03	x
8	-0.01	<b>-0.06***</b>	<b>-0.06***</b>	<b>-0.06***</b>	<b>-0.05***</b>	<b>-0.04**</b>	<b>-0.02+</b>	-0.04	-0.04	0.02	0	-0.02
Kaolinite Index												
	1	2	3	4.1	4.2	4.3	5.1	5.2	5.3	7.1	7.2	7.3
2	-0.01	x										
3	-0.01	0	x									
4.1	0	0.01	0	x								
4.2	0	0.01	0.01	0	x							
4.3	0	0.01	0.01	0	0	x						
5.1	0.01	<b>0.02+</b>	<b>0.02*</b>	0.01	0.01	0.01	x					
5.2	0.01	0.02	0.01	0.01	0.01	0.01	0	x				
5.3	0.01	0.01	0.01	0.01	0	0	-0.01	0	x			
7.1	0.01	<b>0.02+</b>	<b>0.02*</b>	0.01	0.01	0.01	0	0	0.01	x		
7.2	0	0.01	0	0	0	0	-0.01	-0.01	-0.01	-0.01	x	
7.3	0.01	0.01	0.01	0.01	0	0	-0.01	0	0	-0.01	0.01	x
8	0	0.01	0.01	0	0	0	-0.01	-0.01	-0.01	-0.01	0	-0.01
Smectite Index												
	1	2	3	4.1	4.2	4.3	5.1	5.2	5.3	7.1	7.2	7.3
2	<b>-0.04***</b>	x										
3	<b>-0.03***</b>	0.01	x									
4.1	<b>-0.04***</b>	0	-0.01	x								
4.2	<b>-0.03***</b>	0	0	0	x							
4.3	<b>-0.03**</b>	0.01	0	0.01	0.01	x						
5.1	<b>-0.04***</b>	0	-0.01	0	0	-0.01	x					
5.2	<b>-0.04*</b>	0	-0.01	0	0	-0.01	0	x				
5.3	<b>-0.04*</b>	0	-0.01	0	0	-0.01	0	0	x			
7.1	<b>-0.04***</b>	0	-0.01	0	0	-0.01	0	0	0	x		
7.2	<b>-0.04***</b>	0	-0.01	0	0	-0.01	0	0	0	0	x	
7.3	<b>-0.04***</b>	0	-0.01	0	0	-0.01	0	0	0	0	0	x
8	<b>-0.04**</b>	0	-0.01	0	0	-0.01	0	0	0	0	0	0

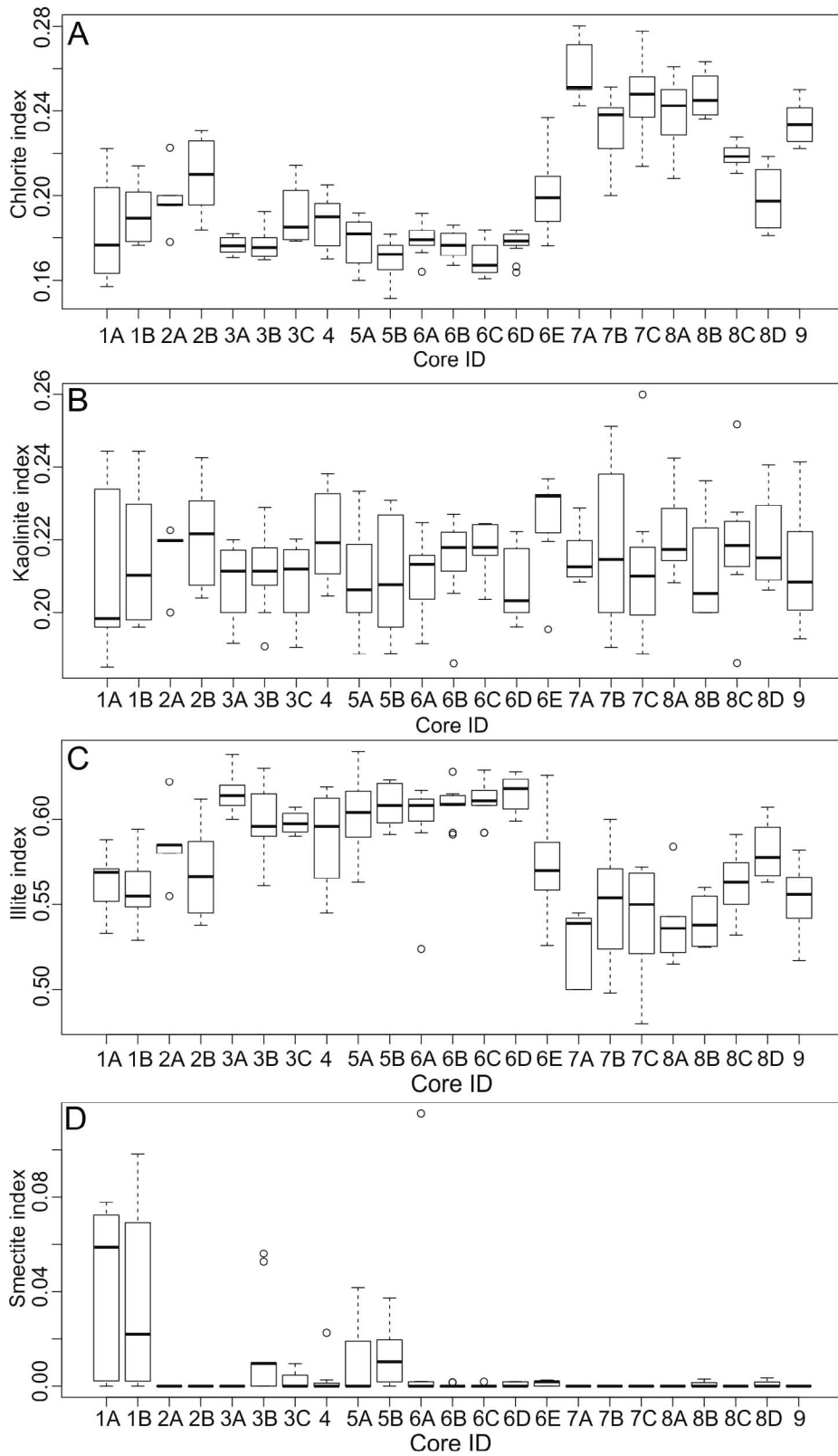


FIG. 19.—Relative clay-mineral abundance as a function of geographic core position (core ID). **A**) Chlorite index, **B**) kaolinite index, **C**) illite index, and **D**) smectite index.



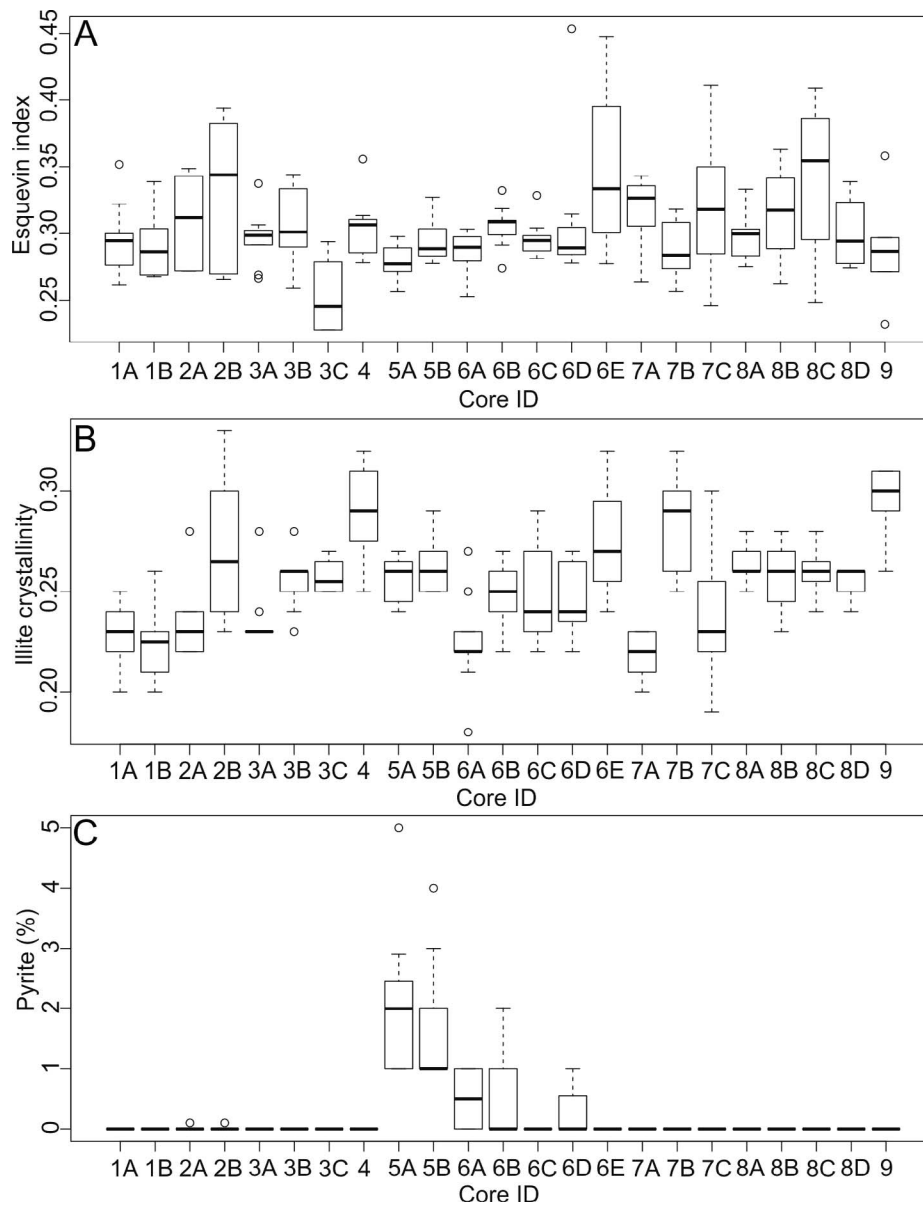


FIG. 20.—Variation in illite chemistry, illite crystallinity, and pyrite abundance as a function of geographic core position (core ID). **A**) Esquevin index, **B**) illite crystallinity, and **C**) pyrite abundance.

is typically present in the finest of all sediment fractions (Fig. 22), and is therefore likely to remain in suspension during transport, and so pass through the Ravenglass Estuary and be deposited offshore (Edzwald and O'Mella 1975; McKinley et al. 2003; Worden and Burley 2003). Second, ground-water flushing (adjustment to the local geochemical environment) has previously been reported to minimize the development and accumulation of smectite (McKinley et al. 2003). It is here speculated that the Ravenglass Estuary might not be a preferential site for smectite accumulation, since metal cations (essential for smectite) might have been flushed from estuarine sediment by twice-daily tides and meteoric groundwater flow through estuarine sediment. However, note that in other estuaries, such as the Gironde estuary, smectite has been deposited on the estuarine floor in clastic sediments (Jouanneau and Latouche 1981).

#### Clay-Mineral Distribution: Early Mineral Alteration (Eodiagenesis)

Both physicochemical processes (Grim and Johns 1954; Griffin and Ingram 1955; Powers 1957; Nelson 1960) and biologically mediated early diagenesis (McIlroy et al. 2003; Needham et al. 2004; Needham et al.

2005; Needham et al. 2006; Worden et al. 2006) have been suggested as potential controls on clay-mineral distribution patterns in sedimentary environments.

The direct ingestion and excretion of sediment by *Arenicola marina* has been shown to lead to clay-mineral alteration and formation under laboratory conditions, due to the chemical conditions in their guts (McIlroy et al. 2003; Needham et al. 2004; Worden et al. 2006). This study has specifically focused on whether bioturbation might have affected clay-mineral distribution patterns in the Ravenglass Estuary. Bioturbation intensity recorded in this study primarily reflects sediment modification by (i) *Arenicola marina*, largely restricted to inner-estuary and central-basin mixed tidal flats (Wooldridge et al. 2017b), that ingest particles < 2 mm in diameter (Riisgard and Banta 1998) and (ii) *Corophium volutator*, confined to mud flats and mixed flats in the Ravenglass Estuary (Kelly et al. 1991), that ingest particles < 62  $\mu$ m in diameter (Fenchel et al. 1975).

In the Ravenglass Estuary, there is a negative correlation between chlorite abundance and bioturbation intensity, and a weak positive correlation between illite abundance and bioturbation intensity (Fig. 21).

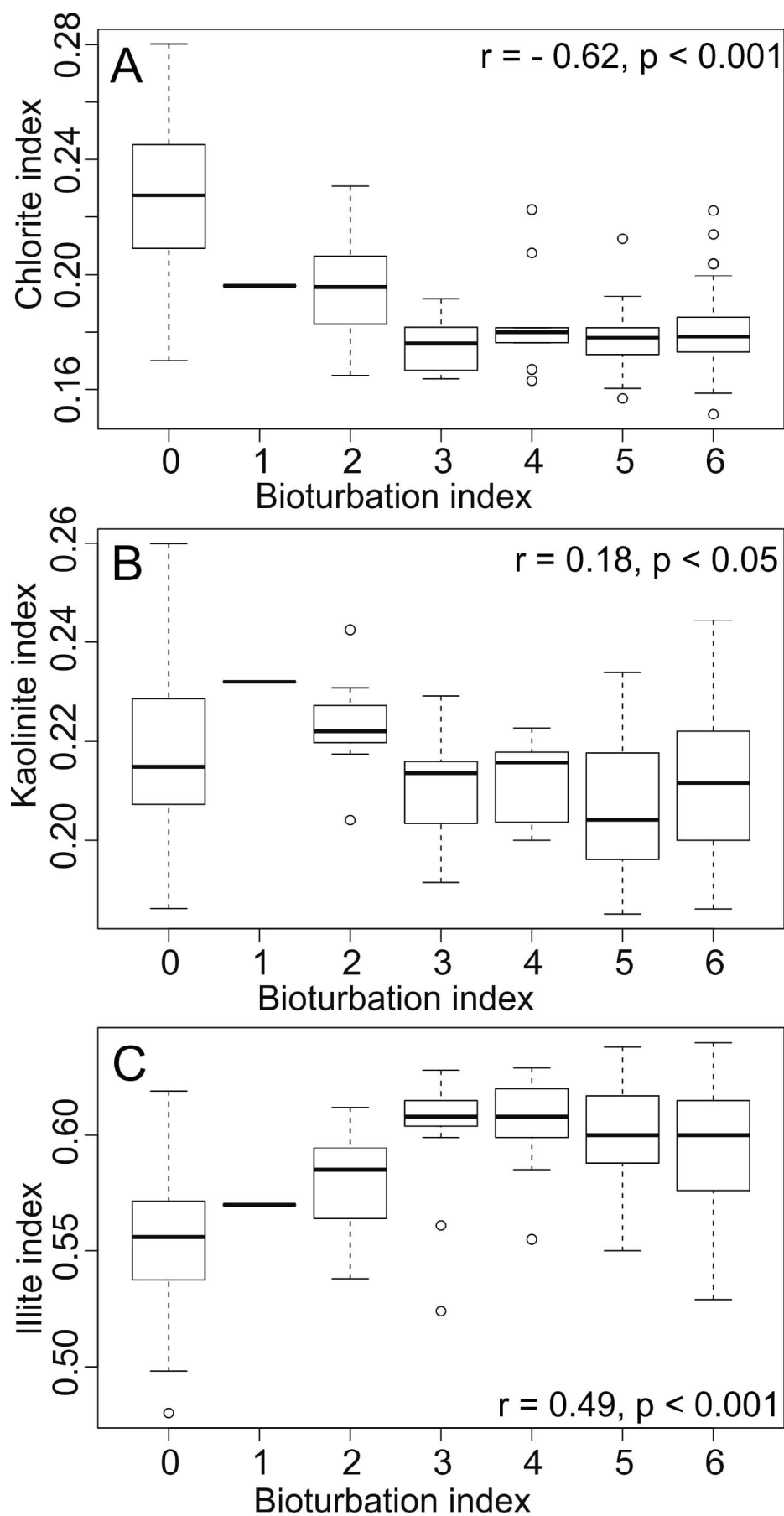


FIG. 21.—Relationship between bioturbation index, after Taylor and Goldring (1993), and relative clay-mineral abundance. **A)** Chlorite index, **B)** kaolinite index, and **C)** illite index. Spearman's correlation coefficients ( $r$ ) between bioturbation index and clay mineral indices are presented, including the level of significance ( $p$ ).



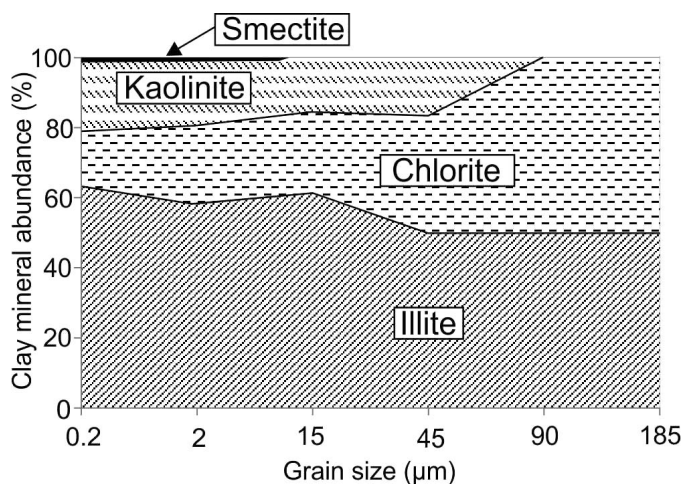


FIG. 22.—Relative abundance of chlorite, illite, kaolinite, and smectite for specific grain-size separate, derived from a single, disaggregated whole sediment sample from the surface of the central basin (Saltcoats). Note that only illite (occurring as flakes) and chlorite (occurring as Fe-rich chlorite lithic grains) are present in grain-size separates greater than 90 µm.

There is little relationship between kaolinite abundance and bioturbation intensity (Fig. 21). The relationships between chlorite and illite abundance and bioturbation intensity is probably an artifact of grain size (Fig. 21), and not early-mineral alteration or formation, since chlorite is most abundant in relatively high-energy, coarser-grained depositional environments barren of bioturbation. In contrast, illite is most abundant in low-energy, finer-grained depositional environments, which are intensely bioturbated by *Corophium volutator* and/or *Arenicola marina*.

Daneshvar and Worden (2018) suggested that plagioclase grains are preferentially rimmed by neoformed kaolinite, and detrital K-feldspar grains are preferentially rimmed by neoformed illite in Ravenglass Estuary sediment, possibly as a result of continued mineral alteration (early diagenesis). While early mineral alteration remains possible, it is reported that clay-minerals also formed due to intense alteration of feldspars in the hinterland (Moseley 1978; Young et al. 1986; Quirke et al. 2015). As a consequence, the relationship between feldspars and clay-minerals in the Ravenglass Estuary plausibly might be an inherited feature from the hinterland, and not due to early diagenesis in the estuary.

#### Clay-Mineral Distribution: Mechanical Infiltration

The stratification of specific clay minerals has been reported to result from the mechanical infiltration of clay-laden waters through filtering sand packages in experiments undertaken by Matlack et al. (1989). Experiments undertaken by Matlack et al. (1989) showed that illite and smectite pass through the sediment but chlorite is preferentially trapped as clay coats. However, the present results from the Ravenglass Estuary show that, despite mechanical infiltration being likely to occur at a centimeter to meter scale in marginal-marine depositional environments (Santos et al. 2012), there is no systematic increase or decrease in specific clay minerals with depth (Table 5).

The lack of clay-mineral stratification in near-surface Ravenglass Estuary sediment brings into question the relevance of experiments undertaken by Matlack et al. (1989) to natural estuarine depositional environments. As reported by Buurman et al. (1998), the infiltration experiments undertaken by Matlack et al. (1989) used peptized clay minerals, i.e., clay minerals converted into a colloidal suspension, meaning that the clay minerals had a minimum tendency to flocculate. As a result, intermediate- to high-surface-charge clay minerals, e.g., illite and smectite,

are less likely to form floccules and are instead more likely to pass through the filtering sand packages (Buurman et al. 1998). In contrast, chlorite (a low-surface-charge clay mineral) is more likely to be trapped in the sediment (Buurman et al. 1998). Second, similarly to the prevention of clay-coat formation via mechanical infiltration (as discussed previously), the formation of clay drapes during flow deceleration and the presence of clay-rich impermeable layers in tidal flats are likely to clog pore throats and baffle mechanical infiltration.

#### Early-Diagenetic Pyrite: Origin and Distribution

Fe-sulfides (e.g., pyrite), are common early-diagenetic minerals in marginal-marine sediments due to bacterial sulfate reduction that occurs when aqueous sulfate (derived from marine inundation) is reduced by organic matter (Berner 1980). In the Ravenglass Estuary, pyrite is most abundant in finer-grained, low-energy, cohesive and anoxic, central-basin tidal flats (Fig. 20C; lithofacies 3, 4.1, and 4.2), typically embedded in detrital-clay coats (Fig. 13B). Pyrite abundance typically increases with depth in tidal-flat cores (cores 6A, 6B, 6D) due to increasing anoxic conditions and the development of a distinct redox boundary, defined by color of sediment at depth typically between 6 to 50 cm (Table 5; Fig. 7). Pyrite is absent throughout the near surface in relatively high-energy and coarser-grained outer-estuary sediment and inner-estuary and central-basin low-amplitude tidal dunes.

The relationship between pyrite abundance and depth is complicated in mixed-flat and low-amplitude-dune depositional environments by sediment bioturbation (Table 5). *Arenicola marina*, which live in J-shaped burrows between 10 to 40 cm deep, develop a tail-to-head-directed ventilatory water flow system causing an upward flow of oxygenated water in the sediment in front of the head (Riisgard and Banta 1998). As a result, the irrigation and oxidation of the burrow by *Arenicola marina* exert a localized but strong effect on the geochemical environment in the near subsurface, in this case, inhibiting the growth of pyrite due to oxidation. In contrast, *Corophium volutator* which live in relatively shallow (< 5 cm deep) U-shaped burrows do not influence pyrite growth, since typically they do not penetrate the redox boundary. It is noteworthy that thin-bedded sediments (lithofacies 4.3), which primarily occur as minor incursions in tidal flats, lead to irrigation and oxidation underlying and overlying sediments, and thus, can also inhibit the growth of pyrite.

#### SIGNIFICANCE: IMPLICATIONS FOR ESTUARINE SANDSTONE RESERVOIR QUALITY

Hydrocarbon exploration, in ancient and deeply buried sandstone reservoirs, typically involves avoiding the cleanest and most clay-free lithofacies. However, note that the cleanest and most clay-free lithofacies tend to become increasingly quartz cemented at burial temperatures > 80 to 100 °C (Worden and Burley 2003). Authigenic clay coats on sand grains can preserve anomalously high porosity by inhibiting quartz cement in deeply buried reservoirs (Ehrenberg 1993). Examples of porosity-preserving authigenic clay coats, in deeply buried marginal-marine sandstone reservoirs, include the Knarr field, northern Norwegian North Sea (Skarpeid et al. 2017) and the Upper Cape Hay Formation, Australia (Saiag et al. 2016). In many reservoir examples, authigenic grain coats have mixed mineralogy, typically containing illite and chlorite (analogous to the Ravenglass Estuary), such as the Egret field (Stricker et al. 2016), the Lower Cretaceous Mississauga Formation (Gould et al. 2010), and the Jurassic Gam Formation (Storvoll et al. 2002).

Authigenic clay coats are reported to form, in sandstones and under laboratory conditions, through the *in situ* growth from the authigenic alteration of precursor and early-diagenetic minerals during burial diagenesis, as well as the thermally driven recrystallization of detrital clay coats (Hillier 1994; Aagaard et al. 2000; Worden and Morad 2003;

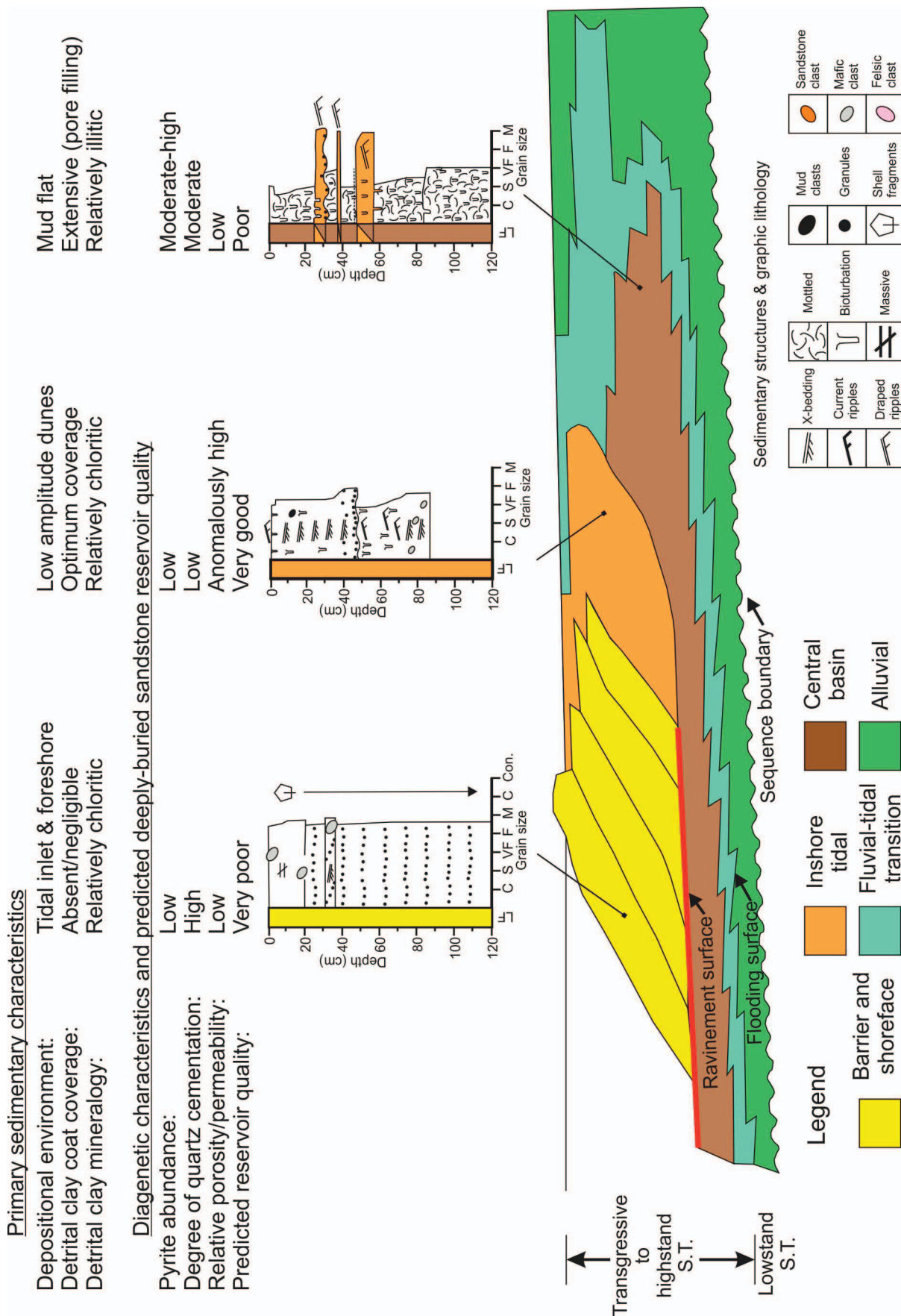


Fig. 23.—Schematic summary of key primary sedimentary and diagenetic characteristics for end-member wave-dominated estuarine depositional environments (facies), as well as predicted reservoir quality for analogous ancient and deeply buried sandstones (temperatures exceeding 80–100°C). The schematic stratigraphic cross-section was modified from Dalrymple et al. (1992).



Ajdkiewicz and Larese 2012). As a result, the spatial distribution of precursor clay minerals, early-diagenetic Fe-sulfide, as well as the extent of detrital-clay-coat coverage in the Ravenglass Estuary, can be used, by analogy, to better predict the distribution of porosity-preserving clay coats in marginal-marine sandstones. The completeness and mineralogy of authigenic clay coats have been reported to be the dominant controls on the ability of grain coats to inhibit quartz cementation (Billault et al. 2003; Lander et al. 2008; Ajdukiewicz and Larese 2012). The optimum grain-coat coverage to preserve porosity varies as a function of grain size, since coarser-grained sandstones have a smaller surface area relative to bulk volume and thus require less clay to achieve full surface coverage (Bloch et al. 2002). For example, Pittman et al. (1992) suggested an optimum range of 4–7% sediment volume as clays for the Berea Sandstone and 5–12% in the Tuscaloosa Formation. In contrast, Bloch et al. (2002) reported that a relatively minor amount of clay (as little as 1–2% of the rock volume) can form extensive coats on individual sand grains.

In the Ravenglass Estuary, detrital clay coats are most extensive at the margins of the inner estuary and the central basin in mud flats (Figs. 15, 23; Table 2); however, the abundance of clay and the fine grain size of the sediment will likely result in detrital and authigenic clay minerals blocking pore throats and drastically reducing permeability. Furthermore, mud flats also contain the highest abundance of pyrite (Fig. 18C), which sequesters iron, and therefore might inhibit the growth of burial-diagenetic authigenic Fe-chlorite, since iron is preferentially locked up as a sulfide mineral. Relatively clean, clay-free, outer-estuarine sediments (Fig. 14) are unlikely to host sufficient quantities of clay-size material to form extensive authigenic clay coats, and would therefore be expected to be heavily quartz cemented during burial diagenesis (at temperatures > 80 to 100 °C). In contrast, low-amplitude tidal dunes, in the inner estuary and the central basin, contain optimum detrital-clay-coat coverage and are relatively enriched in detrital chlorite (Figs. 17A, 19A). Mixed flats in the Ravenglass Estuary contain extensive detrital-clay-coats; however, the sediments are typically depleted in chlorite. Intense bioturbation of low-amplitude-dune and mixed-flat depositional environments (FA 4 and lithofacies 5.1; Table 2), leading to oxidation of near-surface sediment and inhibition of pyrite growth (increasing iron availability), is likely to favor the formation of burial-diagenetic Fe-bearing clay minerals such as chlorite.

## CONCLUSIONS

This study has revealed the dominant controls on distribution patterns of detrital-clay coats and clay minerals, as well as the preferred environments for the growth of Fe-sulfides, in a modern marginal-marine setting. The results of this study can be used, by analogy, to aid prediction of reservoir quality in deeply buried sandstone reservoirs. The main conclusions, which answer the research question stated in the introduction, are summarized below.

In Ravenglass surface (< 2 cm) and near-surface (< 1 m) estuarine sediments, detrital-clay coats are most extensive in mud flats and mixed flats and are almost entirely absent in outer estuarine sediments. Distribution patterns of detrital-clay coats in near-surface (< 1 m) sediment are governed by estuarine hydrodynamics (supply of clay-size material) and attachment of clay minerals to biofilm-coated sand grain surfaces; biofilms are secreted by epipellic diatoms during locomotion in the top few millimeters in the primary depositional environment. Distribution patterns of surface (< 2 cm) detrital-clay coats in the Ravenglass Estuary have not been overprinted by postdepositional processes (e.g., mechanical infiltration or sediment bioturbation) in the near-surface (< 1 m).

The fine fraction (< 2 μm) of Ravenglass Estuary sediment is dominated by Fe-Mg-rich illite, with subordinate amounts of chlorite and kaolinite, with only a trace quantity of smectite. The near-surface clay-mineral assemblage is primarily controlled by provenance and possibly by

the geochemical environment at the site of deposition. Chlorite is most abundant in high-energy, coarser-grained depositional environments, such as outer estuarine sediments and inner-estuary low-amplitude dunes. Kaolinite abundance is relatively homogeneous throughout the Ravenglass Estuary. Illite is typically Fe-Mg-rich and most abundant in mud-flat and mixed-flat inner-estuary and central-basin lithofacies. Relatively high-energy lithofacies in the outer, inner, and central-basin sediments typically host a mixture of both Fe-Mg-rich illite and Al-rich-illite. Smectite is most abundant, but still a minor component in floodplain sediments, and is typically absent in estuarine sediments. Clay-mineral distribution patterns are controlled by estuarine hydrodynamics, due to the physical sorting of clay minerals by grain size. Postdepositional processes, e.g., mechanical infiltration and early-diagenetic mineral alteration via continued weathering of silicate minerals and biodegradation, do not appear to influence clay-mineral distribution patterns in near-surface sediment. However, it might be possible that ground-water flushing in estuarine sediments minimizes the development of smectite accumulation.

Pyrite is the dominant Fe-sulfide in the Ravenglass Estuary. Pyrite growth is largely restricted to mud flats and mixed flats in the central basin, and typically increases in abundance with depth due to increasingly anoxic conditions. Intense bioturbation in mixed flats and low-amplitude dunes by *Arenicola marina* can, however, inhibit pyrite growth (reducing Fe sequestration in the sediment), which might favor the formation of burial-diagenetic chlorite. Distribution patterns of precursor clay coats, clay minerals and Fe-sulfide (pyrite) can be predicted as a function of lithofacies, with knowledge of sediment provenance, estuarine type (resulting hydrodynamics), and the distribution of macrofauna and microfauna.

This modern analogue can be employed to help facilitate reservoir-quality prediction since authigenic clay coats and clay minerals in sandstone reservoirs originate from the thermally driven recrystallization of detrital clay coats or through *in situ* growth from the authigenic alteration of detrital and early-diagenetic minerals during burial diagenesis. Low-amplitude tidal dunes in the inner estuary and the central basin are likely to host the best sandstone reservoir quality due to an optimum detrital-clay-coat coverage, relative chlorite enrichment, and a reduction in Fe-sulfide formation due to intense bioturbation.

## ACKNOWLEDGMENTS

This work was undertaken as part of the Chlorite Consortium at the University of Liverpool, sponsored by BP, Shell, Equinor, Eni, Chevron, Woodside, and Petrobras. We thank Sally Sutton, Benjamin Brigaud, Stuart Jones, Christopher Stevenson, and one anonymous reviewer for their detailed and constructive comments, which have helped improve this manuscript. Special thanks are offered to FEI (now ThermoFisher) for providing the QEMSCAN®, with huge gratitude expressed to Prof Alan Butcher for facilitating this provision.

## REFERENCES

- AAGAARD, P., JAHREN, J.S., HARSTAD, A.O., NILSEN, O., AND RAMM, M., 2000, Formation of grain-coating chlorite in sandstones. Laboratory synthesized vs. natural occurrences: *Clay Minerals*, v. 35, p. 261–269.
- AJDUKIEWICZ, J.M., AND LARESE, R.E., 2012, How clay grain coats inhibit quartz cement and preserve porosity in deeply buried sandstones: observations and experiments: *American Association of Petroleum Geologists, Bulletin*, v. 96, p. 2091–2119.
- ALLEN, G.P., AND POSAMENTIER, H.W., 1994, Transgressive facies and sequence architecture in mixed tide- and wave-dominated incised valleys: example from the Gironde Estuary, France, in Dalrymple, R.W., Boyd, R.J., and Zaitlin, B.A., eds., *Incised Valley Systems: Origin and Sedimentary Sequences*: SEPM, Special Publication 51, p. 225–240.
- AOUDJIT, H., ROBERT, M., ELSASS, F., AND CURMI, P., 1995, Detailed study of smectite genesis in granitic saprolites by analytical electron microscopy: *Clay Minerals*, v. 30, p. 135–147.
- BENJAMINI, Y., AND HOCHBERG, Y., 1995, Controlling the false discovery rate: a practical and powerful approach to multiple testing: *Royal Statistical Society, Journal, Series B (Methodological)*, v. 57, p. 289–300.

- BERNER, R.A., 1980, *Early Diagenesis: A Theoretical Approach*: Princeton, Princeton University Press, 256 p.
- BIDDLE, P., AND MILES, J., 1972, The nature of contemporary silts in British estuaries: *Sedimentary Geology*, v. 7, p. 23–33.
- BILLAULT, V., BEAUFORT, D., BARONNET, A., AND LACHARPAGNE, J.C., 2003, A nanopetrographic and textural study of grain-coating chlorites in sandstone reservoirs: *Clay Minerals*, v. 38, p. 315–328.
- BLOCH, S., LANDER, R.H., AND BONNELL, L., 2002, Anomalous high porosity and permeability in deeply buried sandstone reservoirs: origin and predictability: *American Association of Petroleum Geologists, Bulletin*, v. 86, p. 301–328.
- BLOTT, S.J., AND PYE, K., 2001, GRADISTAT: a grain size distribution and statistics package for the analysis of unconsolidated sediments: *Earth Surface Processes and Landforms*, v. 26, p. 1237–1248.
- BOUSHER, A., 1999, Basic characteristics and evaluation of restoration options, RESTRAT (Restoration Strategies for Radioactively Contaminated Sites and their Close Surroundings): Technical Deliverable, TD12, p. 1–71.
- BROCKAMP, O., AND ZUTHER, M., 2004, Changes in clay mineral content of tidal flat sediments resulting from dike construction along the Lower Saxony coast of the North Sea, Germany: *Sedimentology*, v. 51, p. 591–600.
- BUURMAN, P., JONGMANS, A.G., AND PIJOU, M.D., 1998, Clay illuviation and mechanical clay infiltration: Is there a difference?: *Quaternary International*, v. 51, p. 66–69.
- CAMPBELL, C.V., 1967, Lamina, laminaset, bed and bedset: *Sedimentology*, v. 8, p. 7–26.
- CARR, A.P., AND BLACKLEY, M.W.L., 1986, Implications of sedimentological and hydrological processes on the distribution of radionuclides: the example of a salt marsh near Ravenglass, Cumbria: *Estuarine, Coastal and Shelf Science*, v. 22, p. 529–543.
- CHAMLEY, H., 1989, *Clay Sedimentology*: Berlin, Springer-Verlag, 560 p.
- CHUNG, F.H., 1974a, Quantitative interpretation of X-ray diffraction patterns of mixtures: 1. Matrix-flushing method for quantitative multicomponent analysis: *Journal of Applied Crystallography*, v. 7, p. 519–525.
- CHUNG, F.H., 1974b, Quantitative interpretation of X-ray diffraction patterns of mixtures: 2. Adiabatic principle of X-ray diffraction analysis of mixtures: *Journal of Applied Crystallography*, v. 7, p. 526–531.
- DALRYMPLE, R.W., ZAITLIN, B.A., AND BOYD, R., 1992, Estuarine facies models: conceptual models and stratigraphic implications: *Journal of Sedimentary Petrology*, v. 62, p. 1130–1146.
- DANESHVAR, E., AND WORDEN, R.H., 2018, Feldspar alteration and Fe minerals: origin, distribution and implications for sandstone reservoir quality in estuarine sediments, in Armitage, P.J., Butcher, A., Churchill, J., Csoma, A., Hollis, C., Lander, R.H., Omma, J., and Worden, R.H., eds., *Reservoir Quality Prediction in Sandstones and Carbonates*: Geological Society of London, Special Publication 435, p. 123–139.
- DAVIS, R.A., AND DALRYMPLE, R.W., 2011, *Principles of Tidal Sedimentology*: New York, Springer, 507 p.
- DOWEY, P.J., WORDEN, R.H., UTLEY, J., AND HODGSON, D.M., 2017, Sedimentary controls on modern sand grain coat formation: *Sedimentary Geology*, v. 353, p. 46–63.
- EBERL, D.D., FARMER, V.C., AND BARRER, R.M., 1984, Clay mineral formation and transformation in rocks and soils [and Discussion]: *Royal Society of London, Philosophical Transactions A, Mathematical, Physical and Engineering Sciences*, v. 311, p. 241–257.
- EDZWALD, J.K., AND O'MELLA, C.R., 1975, Clay distributions in recent estuarine sediments: *Clays and Clay Minerals*, v. 23, p. 39–44.
- EIHRENBURG, S.N., 1993, Preservation of anomalously high-porosity in deeply buried sandstones by grain coating chlorite: examples from the Norwegian continental shelf: *American Association of Petroleum Geologists, Bulletin*, v. 77, p. 1260–1286.
- ESQUEVIN, J., 1969, Influence de la composition chimique des illites sur leur cristallinité: *Centre Recherche Elf Pau-SNPA, Bulletin*, v. 3, p. 147–153.
- FENCHEL, T., KOFOED, L.H., AND LAPPALAINEN, A., 1975, Particle size-selection of two deposit feeders: the amphipod *Corophium volutator* and the prosobranch *Hydrobia ulvae*: *Marine Biology*, v. 30, p. 119–128.
- FEUILLET, J.-P., AND FLEISCHER, P., 1980, Estuarine circulation: controlling factor of clay mineral distribution in James River Estuary, Virginia: *Journal of Sedimentary Petrology*, v. 50, p. 267–279.
- GERDOL, V., AND HUGHES, R.G., 1994, Effect of *Corophium volutator* on the abundance of benthic diatoms, bacteria and sediment stability in two estuaries in southeastern England: *Marine Ecology, Progress Series*, p. 109–115.
- GIBBS, R.J., 1977, Clay mineral segregation in the marine environment: *Journal of Sedimentary Petrology*, v. 47, p. 237–243.
- GOULD, K., PE-PIPER, G., AND PIPER, D.J.W., 2010, Relationship of diagenetic chlorite rims to depositional facies in Lower Cretaceous reservoir sandstones of the Scotian Basin: *Sedimentology*, v. 57, p. 587–610.
- GRIFFIN, G.M., AND INGRAM, R.L., 1955, Clay minerals of the Neuse River estuary: *Journal of Sedimentary Petrology*, v. 25, p. 194–200.
- GRIM, R.E., AND JOHNS, W.D., 1954, Clay mineral investigations of sediments in the northern Gulf of Mexico: *Clays and Clay Minerals*, v. 2, p. 81–103.
- GRIM, R.E., BRAY, R.H., AND BRADLEY, W.F., 1937, The mica in argillaceous sediments: *American Mineralogist*, v. 22, p. 813–829.
- HATHAWAY, J.C., 1972, Regional clay mineral fades in estuaries and continental margin of the United States east coast, in Nelson, B.W., ed., *Environmental Framework of Coastal Plain Estuaries*: Geological Society of America, Memoir 133, p. 293–316.
- HILLIER, S., 1994, Pore-lining chlorites in siliciclastic reservoir sandstones: electron microprobe, SEM and XRD data, and implications for their origin: *Clay Minerals*, v. 29, p. 665–680.
- JONES, S.J., 2017, Goo, glue, and grain binding: importance of biofilms for diagenesis in sandstones: *Geology*, v. 45, p. 959–960.
- JOUANNEAU, J.-M., AND LATOUCHE, C., 1981, The Gironde Estuary: Contributions to *Sedimentary Geology*, v. 10, 115 p.
- KELLY, M., EMPTAGE, M., MUDGE, S., BRADSHAW, K., AND HAMILTON-TAYLOR, J., 1991, The relationship between sediment and plutonium budgets in a small macrotidal estuary: Esk Estuary, Cumbria, UK: *Journal of Environmental Radioactivity*, v. 13, p. 55–74.
- KÜBLER, B., 1964, Les argiles, indicateurs de métamorphisme: *Review Institute Français du Pétrole*, v. 19, p. 1093–1112.
- LANDER, R.H., LARESE, R.E., AND BONNELL, L.M., 2008, Toward more accurate quartz cement models: the importance of euhedral versus noneuhedral growth rates: *American Association of Petroleum Geologists, Bulletin*, v. 92, p. 1537–1563.
- LOYD, J.M., ZONG, Y., FISH, P., AND INNES, J.B., 2013, Holocene and Late Glacial relative sea-level change in north-west England: implications for glacial isostatic adjustment models: *Journal of Quaternary Science*, v. 28, p. 59–70.
- MATLACK, K.S., HOUSEKNECHT, D.W., AND APPLIN, K.R., 1989, Emplacement of clay into sand by infiltration: *Journal of Sedimentary Petrology*, v. 59, p. 77–87.
- MCDUGALL, D.A., 2001, The geomorphological impact of Loch Lomond (Younger Dryas) Stadial plateau icefields in the central Lake District, northwest England: *Journal of Quaternary Science*, v. 16, p. 531–543.
- MCILROY, D., WORDEN, R.H., AND NEEDHAM, S.J., 2003, Faeces, clay minerals and reservoir potential: *Geological Society of London, Journal*, v. 160, p. 489–493.
- MCINLEY, J.M., WORDEN, R.H., AND RUFFELL, A.H., 2003, Smectite in sandstones: a review of the controls on occurrence and behaviour during diagenesis, in Worden, R.H., and Morad, S., eds., *Clay Mineral Cements in Sandstones*: International Association of Sedimentologists, Special Publication 34, p. 109–128.
- MEADE, R.H., 1969, Landward transport of bottom sediments in estuaries of the Atlantic coastal plain: *Journal of Sedimentary Petrology*, v. 39, p. 222–234.
- MERRITT, J.W., AND AUTON, C.A., 2000, An outline of the lithostratigraphy and depositional history of Quaternary deposits in the Sellafield district, west Cumbria: *Yorkshire Geological Society, Proceedings*, v. 53, p. 129–154.
- MOORE, D.M., AND REYNOLDS, R.C., 1997, *X-Ray Diffraction and the Identification and Analysis of Clay Minerals*: Oxford, U.K., Oxford University Press, 378 p.
- MORAD, S., AL-RAMADAN, K., KETZER, J.M., AND DE ROS, L.F., 2010, The impact of diagenesis on the heterogeneity of sandstone reservoirs: a review of the role of depositional facies and sequence stratigraphy: *American Association of Petroleum Geologists, Bulletin*, v. 94, p. 1267–1309.
- MORAES, M.A.S., AND DE ROS, L.F., 1990, Infiltrated clays in fluvial Jurassic sandstones of Recôncavo Basin, northeastern Brazil: *Journal of Sedimentary Petrology*, v. 60, p. 809–819.
- MOSELEY, F., 1978, *The Geology of the Lake District*, Yorkshire Geological Society, 284 p.
- NEEDHAM, S.J., WORDEN, R.H., AND MCILROY, D., 2004, Animal–sediment interactions: the effect of ingestion and excretion by worms on mineralogy: *Biogeosciences*, v. 1, p. 113–121.
- NEEDHAM, S.J., WORDEN, R.H., AND MCILROY, D., 2005, Experimental production of clay rims by macrobiotic sediment ingestion and excretion processes: *Journal of Sedimentary Research*, v. 75, p. 1028–1037.
- NEEDHAM, S.J., WORDEN, R.H., AND CUADROS, J., 2006, Sediment ingestion by worms and the production of bio-clays: a study of macrobiologically enhanced weathering and early diagenetic processes: *Sedimentology*, v. 53, p. 567–579.
- NELSON, B.W., 1960, Clay mineralogy of the bottom sediments, Rappahannock River, Virginia: *Clays and Clay Minerals, Seventh National Conference, Proceedings*, p. 135–148.
- OELKERS, E.H., BJORKUM, P.A., AND MURPHY, W.M., 1996, A petrographic and computational investigation of quartz cementation and porosity reduction in North Sea sandstones: *American Journal of Science*, v. 296, p. 420–452.
- PITTMAN, E.D., LARESE, R.E., AND HEALD, M.T., 1992, Clay coats: occurrence and relevance to preservation of porosity in sandstones, in Houseknecht, D.W., and Pittman, E.D., eds., *Origin, Diagenesis, and Petrophysics of Clay Minerals in Sandstones*: SEPM, Special Publication 47, p. 241–255.
- POSTMA, H., 1967, Sediment transport and sedimentation in the estuarine environment, in Lauff, G.H., ed., *Estuaries*: Washington, D.C., American Association for the Advancement of Science, p. 158–184.
- POWERS, M.C., 1957, Adjustment of land derived clays to the marine environment: *Journal of Sedimentary Petrology*, v. 27, p. 355–372.
- QUIRKE, J., HENDERSON, C.M.B., PATRICK, R.A.D., ROSSO, K.M., DENT, A., SHARPLES, J.W., AND PEARCE, C.I., 2015, Characterizing mineralogy and redox reactivity in potential host rocks for a UK geological disposal facility: *Mineralogical Magazine*, v. 79, p. 1353–1367.
- R CORE TEAM, 2016, R: a language and environment for statistical computing: R Foundation for Statistical Computing, Vienna, Austria.
- RATEEV, M.A., SADCHIKOVA, T.A., AND SHABROVA, V.P., 2008, Clay minerals in recent sediments of the World Ocean and their relation to types of lithogenesis: *Lithology and Mineral Resources*, v. 43, p. 125–135.
- REINECK, H.-E., AND WUNDERLICH, F., 1968, Classification and origin of flaser and lenticular bedding: *Sedimentology*, v. 11, p. 99–104.

- RISGARD, H.U., AND BANTA, G.T., 1998, Irrigation and deposit feeding by the lugworm *Arenicola marina*, characteristics and secondary effects on the environment: a review of current knowledge: *Vie et Milieu*, v. 48, p. 243–258.
- RUDERT, M., AND MÜLLER, G., 1981, Mineralogy and provenance of suspended solids in estuarine and near-shore areas of the southern North Sea: *Senckenbergiana Maritima*, v. 13, p. 57–64.
- SAIAG, J., BRIGAUD, B., PORTIER, E., DESAUBLIAUX, G., BUCHERIE, A., MISKA, S., AND PAGEL, M., 2016, Sedimentological control on the diagenesis and reservoir quality of tidal sandstones of the Upper Cape Hay Formation (Permian, Bonaparte Basin, Australia): *Marine and Petroleum Geology*, v. 77, p. 597–624.
- SALEM, A.M., MORAD, S., MATO, L.F., AND AL-AASM, I.S., 2000, Diagenesis and reservoir-quality evolution of fluvial sandstones during progressive burial and uplift: evidence from the Upper Jurassic Boipeba Member, Reconcavo basin, northeastern Brazil: *American Association of Petroleum Geologists, Bulletin*, v. 84, p. 1015–1040.
- SANTOS, I.R., EYRE, B.D., AND HUETTEL, M., 2012, The driving forces of porewater and groundwater flow in permeable coastal sediments: a review: *Estuarine, Coastal and Shelf Science*, v. 98, p. 1–15.
- SIMPSON, B., 1934, The petrology of the Eskdale (Cumberland) granite: The Geologists' Association, *Proceedings*, v. 45, p. 17–34.
- SKARPEID, S.S., CHURCHILL, J.M., HILTON, J.P.J., IZATT, C.N., AND POOLE, M.T., 2017, The Knarr Field: a new development at the northern edge of the North Sea: *Geological Society of London, Petroleum Geology Conference Series*, v. 8, p. 445–454.
- STORVOLL, V., BJØRLYKKE, K., KARLSEN, D., AND SAIGAL, G., 2002, Porosity preservation in reservoir sandstones due to grain-coating illite: a study of the Jurassic Garn Formation from the Kristin and Lavrans fields, offshore Mid-Norway: *Marine and Petroleum Geology*, v. 19, p. 767–781.
- STRICKER, S., JONES, S.J., SATHAR, S., BOWEN, L., AND OXTOBY, N., 2016, Exceptional reservoir quality in HPHT reservoir settings: examples from the Skagerrak Formation of the Heron Cluster, North Sea, UK: *Marine and Petroleum Geology*, v. 77, p. 198–215.
- TAYLOR, A.M., AND GOLDRING, R., 1993, Description and analysis of bioturbation and ichnofabrics: *Geological Society of London, Journal*, v. 150, p. 141–148.
- UK ENVIRONMENTAL AGENCY, 2015, LIDAR Composite DTM, <https://data.gov.uk/dataset/lidar-composite-dtm-1m1>.
- UNDERWOOD, G.J.C., AND PATERSON, D.M., 1993, Seasonal changes in diatom biomass, sediment stability and biogenic stabilization in the Severn Estuary: *Marine Biological Association of the United Kingdom, Journal*, v. 73, p. 871–887.
- WHITEHOUSE, U.G., JEFFREY, L.M., AND DEBBRECHT, J.D., 1960, Differential settling tendencies of clay minerals in saline waters: *Clays and Clay Minerals*, v. 7, p. 1–79.
- WILSON, M.D., 1992, Inherited grain-rimming clays in sandstones from eolian and shelf environments: their origin and control on reservoir properties, in Houseknecht, D.W. and Pittman, E.D., eds., *Origin, Diagenesis and Petrophysics of Clay Minerals in Sandstones*: SEPM, Special Publication 47, p. 209–225.
- WOOLDRIDGE, L.J., WORDEN, R.H., GRIFFITHS, J., THOMPSON, A., AND CHUNG, P., 2017a, Biofilm origin of clay-coated sand grains: *Geology*, v. 45, p. 875–878.
- WOOLDRIDGE, L.J., WORDEN, R.H., GRIFFITHS, J., AND UTLEY, J.E.P., 2017b, Clay-coated sand grains in petroleum reservoirs: understanding their distribution via a modern analogue: *Journal of Sedimentary Research*, v. 87, p. 338–352. doi:10.2110/jsr.2017.20
- WOOLDRIDGE, L.J., WORDEN, R.H., GRIFFITHS, J., UTLEY, J.E.P., AND THOMPSON, A., 2018, The origin of clay-coated sand grains and sediment heterogeneity in tidal flats: *Sedimentary Geology*, v. 373, p. 1910–209.
- WORDEN, R.H., AND BURLEY, S.D., 2003, Sandstone diagenesis: the evolution from sand to stone, in Burley, S.D. and Worden, R.H., eds., *Sandstone Diagenesis: Recent and Ancient*: International Association of Sedimentologists, Reprint Series, v. 4, p. 3–44.
- WORDEN, R.H., AND MORAD, S., 2003, Clay minerals in sandstones: controls on formation, distribution and evolution, in Worden, R.H., and Morad, S., eds., *Clay Mineral Cements in Sandstones*: International Association of Sedimentologists, Special Publication 34, p. 3–41.
- WORDEN, R.H., NEEDHAM, S.J., AND CUADROS, J., 2006, The worm gut: a natural clay mineral factory and a possible cause of diagenetic grain coats in sandstones: *Journal of Geochemical Exploration*, v. 89, p. 428–431.
- WORDEN, R., ARMITAGE, P., BUTCHER, A., CHURCHILL, J., CSOMA, A., HOLLIS, C., LANDER, R., AND OMMMA, J., 2018, Petroleum reservoir quality prediction: overview and contrasting approaches from sandstone and carbonate communities, in Armitage, P.J., Butcher, A., Churchill, J., Csoma, A., Hollis, C., Lander, R.H., Omma, J., and Worden, R.H., eds., *Reservoir Quality Prediction in Sandstones and Carbonates*: Geological Society of London, Special Publication 435, p. 1–31.
- YOUNG, B., FORTEY, N.J., AND NANCARROW, P.H.A., 1986, An occurrence of tungsten mineralisation in the Eskdale Intrusion, West Cumbria: *Yorkshire Geological Society, Proceedings*, v. 46, p. 15–21.

Received 18 January 2018; accepted 29 June 2018.